Tailoring shape, size and optical properties of gold and silver nanostructures for bio-medical applications

A thesis submitted towards the partial fulfilment of BS-MS programme

(2014-2019)

By

Amar Alok

20141013

Under the guidance of

Prof. Nadine Millot & Dr. Lionel Maurizi

Laboratoire Interdisciplinaire Carnot de Bourgogne

Université de Bourgogne

Dijon, France

Certificate

This is to certify that this dissertation titled '**Tailoring shape, size and optical properties of gold and silver nanostructures for bio-medical applications**' towards the partial fulfilment of the BS-MS dual degree programme at the Indian Institute of Science Education and Research, Pune represents study/work carried out by **Amar Alok** under the supervision of **Prof. Nadine Millot** and **Dr. Lionel Maurizi**, BH2N group, Laboratoire Interdisciplinaire Carnot de Bourgogne, Dijon, France during the academic year, 2018-2019.

Amar Alok

20141013

IISER Pune

Prof. Nadine Millot

Head of BH2N team

Nanoscience department

Laboratoire Interdisciplinaire Carnot de Bourgogne

Dijon, FRANCE

21000

E-mail: nadine.millot@u-bourgogne.fr

Dr. Lionel Maurizi

CNRS Researcher

BH2N team, Nanoscience department

Laboratoire Interdisciplinaire Carnot de Bourgogne

Dijon, FRANCE

21000

E-mail: lionel.maurizi@u-bourgogne.fr

Date : 01-04-2019

Declaration

I hereby declare that the matter embodied in the report titled '**Tailoring shape, size and optical property of gold and silver nanostructures for bio-medical applications**' are the results of the work carried out by me at Laboratoire Interdisciplinaire Carnot de Bourgogne, Dijon, France, under the supervision of **Prof. Nadine Millot** and **Dr. Lionel Maurizi** during the academic year 2018-2019 and the same has not been submitted elsewhere.

Signature of Student

Amar Alok

Signature of Thesis Supervisor

Prof. Nadine Millot **Dr. Lionel Maurizi**

Date:

Place:

Acknowledgments

Once I begin to write a few lines on this blank page, I understand that my stay at ICB is about to end. This long journey could not have such a great and transformative significance for me without the support of several people.

First of all, I wish to express my sincere gratitude to my supervisors Prof. Nadine Millot, Dr. Lionel Maurizi and Dr. Lucien Saviot for their every suggestion which was meaningful, even though, in some cases, I understood later. I am always inspired by their transparent way of expressing scientific questions. My motivation is partly derived by their scientific efforts and enthusiasm towards the research.

It has been a great privilege to be guided in my every step by Prof. Stephane Guerin. I send my hearty thanks to him for inspiring me constantly during my stay in Dijon, which led to the accomplishment of the present thesis. I am also very much grateful to Dr. Julien Boudon for helping me with the characterization issues by giving me thorough advice.

I pass my best regards to my previous mentors Prof. Satishchandra Ogale and Dr. Ashna Bajpai at IISER Pune who showed me the way into the world of material science. Also, I must acknowledge Prof. Deepak Dhar, my local supervisor at IISER Pune for his valuable assertions and motivation during my master's thesis. I owe my gratitude to all faculty members of the Physics and Chemistry Department at IISER Pune for their comprehensive teaching during my academic program, which has increased my knowledge in the field of material science.

I have no words to express my profound appreciation to my friends, especially Maria Doina Craciun and Stefania Emilia Diaconu, for their prompt help in the neat making of this project. I am overwhelmed by their inspiring guidance, constructive criticism, pragmatic solutions, kind hospitality and unconditional love towards me.

Acknowledgments seem to be incomplete without a word of thanks to my father Prof. Satishchandra Bharati, my mother Prof. Snehlata Bharati and my sister Er. Shalu Priya whose blessings and patience pushed me to make my ideas into practice and give the best of myself in every situation. Above all, I thank Lord Shiva who enabled me with the mind, strength, and determination to present this work.

Amar Alok

Dedicated to Lord Shiva

Contents

List of Figures

List of Tables

List of abbreviations

NPs	Nanoparticles
NRs	Nanorods
UV-vis	Ultraviolet-visible
EDS	Energy-dispersive X-ray Spectroscopy
TEM	Transmission Electron Microscopy
STEM	Scanning Transmission Electron Microscopy
HRTEM	High-Resolution Transmission Electron Microscopy
SAED	Selected Area Electron Diffraction
SPR	Surface Plasmon Resonance
EM	Electromagnetic
LSPR	Localized Surface Plasmon Resonance
NIR	Near Infrared
ICDD	International Centre for Diffraction Data
CTAB	Cetyl trimethylammonium bromide
DI	Deionized
PdI	Polydispersity Index

Abstract

Nanostructures of gold and silver (nanospheres, nanorods, and core-shell nanostructures) are considered to be the workhorse of next generation nanomedicine. They can be synthesized in different shapes and sizes with controlled dispersity and easy functionalization with specific antibodies and targeting agents. Faraday studied colloidal gold and the optical properties of metal NPs. Since then many studies were made that leads to improvements in classical wet chemistry methods for synthesis of noble metal NPs. They are found as atomic clusters in the colloidal suspension and exhibit different optical properties depending on their size and structure. The different parameters that influence the size, growth, and dispersion of gold and silver NPs are studied. The optical and electromagnetic field enhancement of these nanostructures can be tailored by fine-tuning their shape and size. This master project aims at the development of multifunctional nano-platform of gold and silver nanostructures targeting potential applications in medical imaging and therapy. To fine-tune the shape, size and optical properties of gold and silver nanostructures, we plan to synthesize metallic NPs and modify their surface with small organic molecule providing different chemical properties (charge, affinities etc.). The conventional Frens-Turkevich synthesis method was used with some modifications. These nanohybrids were characterized via analytical methods such as DLS, UV-vis and electron microscopy to develop, optimize and control biocompatible synthesis.

Experiments were made by changing one parameter at a time like the metal precursor concentration and the citrate concentration followed by the spectroscopic characterization to optimize the synthesis. Nanostructures of gold and silver such as Au NRs and Ag-Au alloy NPs were also synthesized to cover the spectra from visible to NIR region. The correlation between the optical properties and the different parameters involved in the synthesis was explored. The optical properties of each nanostructure were studied by analyzing their absorption spectra.

DLS, UV-vis spectra, EDS, TEM, STEM, HRTEM and SAED images were used to determine the size, shape, dispersion, optical property, elemental composition and crystallographic analysis of the colloid NPs.

Chapter 1

1.1 Introduction

Nanotechnology is one of the quickest developing fields in science and engineering. Some of the most noticeable examples of nanomaterials are noble metal nanostructures, such as nanoparticles (NPs) [1]–[4], nanorods [5]–[7], nanowires, nanotriangles, nanostars, core-shell and homogeneously alloyed nanostructures [8], [9] and many others. Half of the gold and silver that come out of mines are used to make jewelry [10]. It has been used in this way for thousands of years. But, researchers have been using the tiny amount of these precious metals in technology and medicine [2]–[4], [7], [11]–[13]. These metals are quite inert in bulk form, but their properties change drastically when scaled down to nanometer length scale (~1-100 nm). This is because of the contribution of the surface atoms is bigger, it leads to significant change in properties, and has to be taken into consideration [14]. In bulk form, surface atoms are negligible compared to bulk atoms. When scaled down to ~50 nm, the size of a virus, the surface atoms of gold NPs can form covalent bonds with specific drug molecules [15]. The high surface area to volume ratio makes them good candidates for drug delivery vehicles. Their surface electrons show quite interesting properties when interacting with light [16]. When the light of correct wavelength is used, free electrons of the conduction band of metal can be made to oscillate collectively at the same frequency which results in enhanced near field amplitude. This special property is called **Surface Plasmon Resonance (SPR)** which makes them precise cancer killers [4], [7], [13]. The antibodies attached to gold NPs can target the tumor cells [4]. When infrared light is shined to these NPs, surface electrons strongly absorb light due to the SPR which then decay into heat that can be used to kill the tumor cells [7]. Silver NPs show superior plasmonic properties and are reported for their antimicrobial properties [3], [17]. On the other hand, Ag-Au alloy NPs retain the noteworthy plasmonic properties of Ag component and the inertness with controlled shape, size, and dispersion of the correspondent Au which grant enhanced chemical stability [9]. The plasmonic properties of these NPs are very sensitive to their size, shape, composition, surface science and environmental conditions [9].

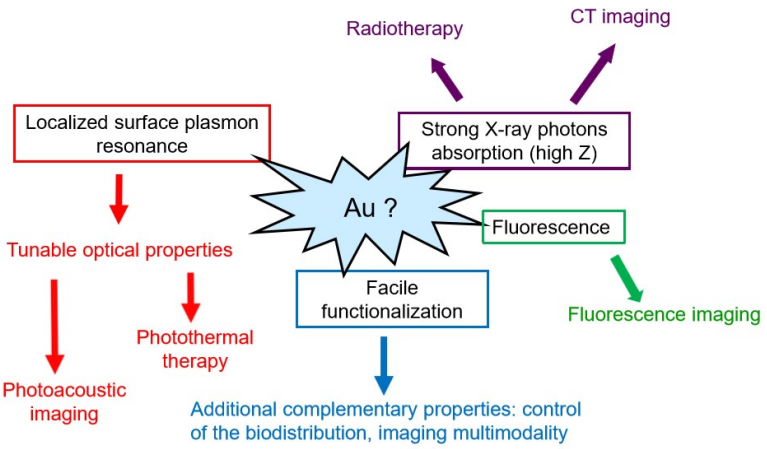

Fig. 1.1: Schematic of bio-medical applications of gold based nanostructures with tunable optical characterstics and facile functionalization.

In 1908, Mie gave a simple, exact solution to Maxwell's equations that govern the extinction spectra (scattering+absorption) of plane EM waves by spherical particles of arbitrary size. The essential point of Mie theory is to find the efficiency coefficients for absorption (Q_a), scattering (Q_s) and extinction (Q_e) which is the ratio of the cross-section (σ_i) for the relevant process to the area of spherical particle taken into consideration. The extinction cross section of a single spherical metal NPs is calculated in terms of the complex dielectric function of the metal ($\varepsilon'(\lambda) + i\varepsilon''(\lambda)$) and the dielectric constant of the medium (ε_m) [18].

$$C_{ext}(\lambda) = \frac{24\pi^2 R^3 \varepsilon_m^{3/2}}{\lambda} \frac{\varepsilon''(\lambda)}{(\varepsilon'(\lambda) + 2\varepsilon_m) + \varepsilon''(\lambda)^2}$$

Where λ refers to the wavelength of the incident light and R is the particle radius

Most of the standard nanoparticle synthesis follow a classical wet chemical method which yield spherical particles. To characterize their spectra, we need to probe a large ensemble of these particles. Hence, Mie theory prediction works reasonably well to describe our results for spherical particles [19]. However, with the help of modern numerical and computational techniques, one can determine the optical properties for non-spherical particles. Plasmonics is a new technology which aims at controlling surface plasmons that result from the interaction between EM waves and the conduction electrons at a metal interface. This interaction is responsible for their vibrant color. Plasmon defines a quantum of plasma oscillation i.e. the quantization of the collective longitudinal excitation of a conductive electron gas [20]. Au NP solution are usually brilliant red and Ag NP solutions are typically yellow.

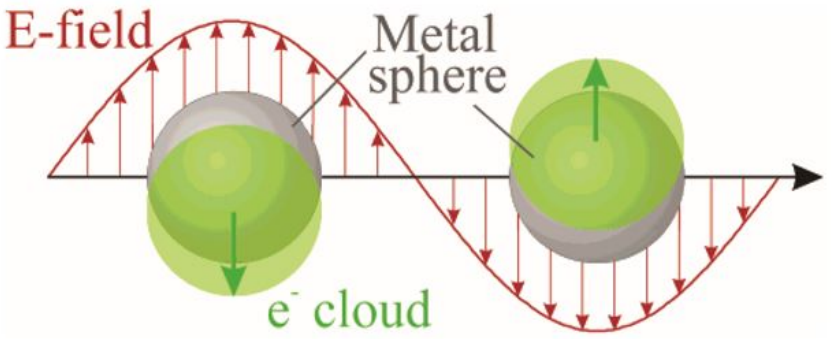

©J. Phys. Chem. B, Vol. 107, No. 3, 2003

Fig. 1.2: Schematic of surface plasmon oscillations by a spherical metal sphere from the interaction between EM waves and the electron cloud.

The metal nanoparticle optical properties depend on several factors including the presence of the metal precursor, solvent layer, electromagnetic coupling of the agglomerated nanoparticles and so on. Hence, it is necessary to understand the electrodynamics of nanoparticles in a complex dielectric environment. In a dielectric material, the electric field causes charge to separate leading to the formation of discrete dipoles whose distance depend on the dielectric properties of the metal and the medium [18]. The phenomenon of SPR can be treated similarly to mass-spring harmonic oscillator but the driving force for SPR is the resonant energy radiation [21]. The resonance condition, in this case, is achieved when the radiation frequency of incident EM wave matches the oscillating frequency of the conduction electrons. The mathematical expression of localized SPR for a metal is expressed as:

$$\omega_{sp} = \sqrt{\frac{\omega_p^2}{1 + 2\varepsilon_m} - \gamma^2}$$

$$\omega_{p} = \sqrt{\frac{Ne^2}{\varepsilon_0 m}}$$

Where, ω_{sp} is the surface plasmon frequency, ω_p is the bulk plasma oscillation frequency, ε_m is the dielectric constant of the medium, γ is the line width of surface plasmon band, N is the density of free carriers, m is the mass of the charge carrier.

1.2 Bio-medical applications

Today, challenges in the bio-medical fields are tremendous and extremely many. This involves the early diagnosis of diseases, tumor localization and treatment, drug delivery, cell imaging, and tracking. The application of nanotechnology for diagnosis, monitoring, treatment, and control of biological structures is alluded to as “nanomedicine” [22]. Gold and silver nanostructures show enhanced permeability and retention effect in tumor tissue compared to normal tissue [4], [7]. Moreover, their high surface area to volume ratio makes them a good candidate for drug delivery vehicles. Multi-functionality helps in the realization of diverse functional traits of nanoparticles. Ag NPs are well known for stronger and sensitive SPR properties, but it is challenging to synthesize them in uniform shapes. They are known for their antimicrobial properties to battle against microorganisms like bacteria fungi and yeasts. They release silver ions that act as a biocidal substance. Silver NPs show a much greater biocidal activity because of their high surface area to volume ratio [17]. On the other hand, Au NPs can be synthesized easily with better control on shape, size and dispersity in a dielectric environment that results in a fine-tuning of the plasmonic property of metal nanoparticles. The strongly enhanced SPR scattering and absorption from Au NPs make them useful as bright optical labels for molecular specific biological imaging and selective laser photothermal therapy for cancer respectively [13]. With the aim to develop multi-functional nanoplatforms for bio-medical applications, we tried to synthesize and characterize Ag NPs, Au NPs, Au NRs and homogenously alloyed Ag-Au alloy nanostructures [9], [23], [24].

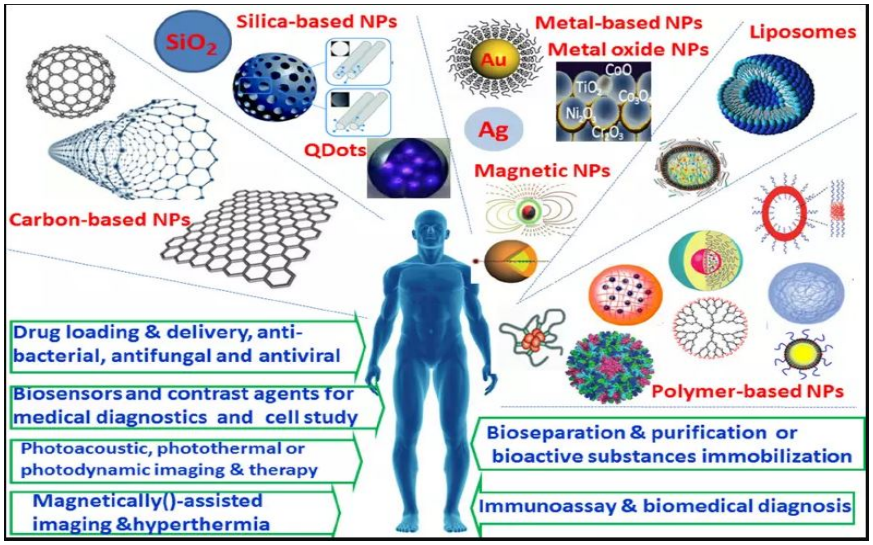

Fig. 1.3: Examples of typical NPs and their bio-medical applications. Metal-based NPs are used for drug delivery and photothermal therapy.

Chapter 2

2.1 State of the Art: Gold & Silver NPs Synthesis (Shapes, sizes and surface chemistry)

Synthesis of Au/Ag nanoparticles can be accomplished by both "top-down" and "bottom-up" approaches. For "top-down" methodology, a bulk Au/Ag is systematically broken down to create NPs of the desired shape and size. In this situation, particle assembly and formation is controlled by a pattern or framework. The "top-down" strategy is always constrained regarding the control of the shape and size of particles as well as in further functionalization [25]. In contrast, for "bottom-up" method, the development of NPs originates from individual molecules which involve a chemical or biological reduction [2], [3], [6], [7]. The chemical reduction method includes two stages: nucleation and successive growth. When the nucleation and successive growth are finished in the same process, it is classified as "in situ synthesis" [9]; else, it is called "seed-growth method" [5], [6].

2.1.1 In Situ Synthesis

The in situ synthesis of NPs involve chemical reduction of gold/silver precursor ($HAuCl_4/AgNO_3$) using agents such as borohydrides, hydroxylamine, hydrazine, , unsaturated and saturated alcohols and stabilization by agents such as trisodium citrate dihydrate, phosphorus ligands, sulfur ligands, oxygen-based ligands, nitrogen-based ligands, dendrimers, and polymers [26]. NPs synthesized by in situ synthesis, can be used for the seed-mediated growth or further functionalization. However, to control the shape and size of in situ synthesized gold NPs is difficult.

2.1.2 Seed-Growth Method

NPs of controllable size and different shapes like nanospheres, nanorods, nanostars, nanocages and so on can be synthesized using seed growth method [5], [6]. Different shapes of NPs can be obtained with variation of the reaction conditions. The seed-mediated synthesis of Au/Ag NPs involves preparation of small-size NP seeds that is then added to a "growth" solution containing gold/silver precursor, stabilizing and reducing agent. The reducing agent used in the growth solution is always milder and the newly reduced gold grows on the seed surface. The seeds act as catalysts inhibiting new particle nucleation to occur in solution [27].

2.2 Experimental Section

The 'in situ synthesis' of the gold and silver spherical NPs described in this report was carried out by using the conventional Frens-Turkevich synthesis method [1] and $NaBH_4$ is used as a strong reducing agent, known as the Brust method. The synthesis is done by the reduction of a solution of chloroauric acid ($HAuCl_4.3H_2O$) and silver nitrate ($AgNO_3$) with sodium borohydride ($NaBH_4$) to obtain NPs of gold and silver respectively. Trisodium citrate is used as a stabilizing agent in order to prevent the agglomeration of NPs and chemisorption of undesired functional groups/proteins on the NP's surface [2]. In previous studies Kamat et al., 1998 [28], used a similar synthesis protocol without the sodium borohydride. The additional use of sodium borohydride as a reductant can provide smaller size gold/silver nanoparticles [9]. Gold nanorods and homogenously alloyed gold and silver nanostructures were synthesized using a seed-mediated growth method.

$$HAuCl_4.3H_2O + NaBH_4 \xrightarrow{25°C} Au + BH_4 + HCl + NaCl_3$$

$$AgNO_3 + NaBH_4 \xrightarrow{25°C} Ag + BH_3 + HNO_3 + NaNO_3$$

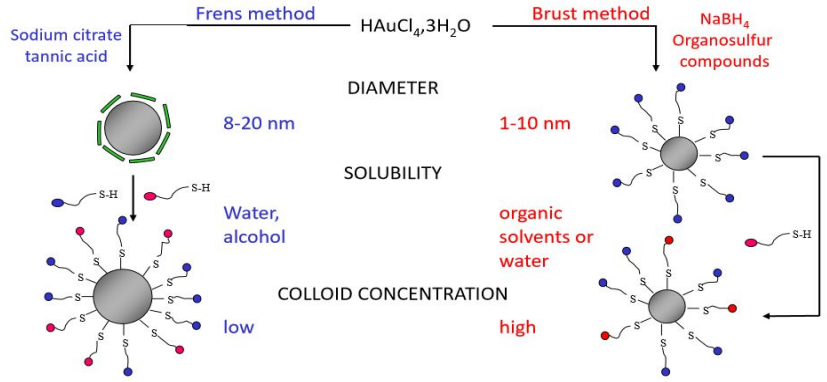

Fig. 2.1: Schematic of Frens-Turkevich synthesis method and Brust method showing the two different size of synthesized NPs. A combination of both methods was used to optimize the synthesis.

2.2.1 Materials and Reagents

$HAuCl_4.3H_2O$ (99.99%, 393.83 a.m.u.), $AgNO_3$ (99%, 169.87 a.m.u.), Tri-sodium citrate dehydrate (294.10 a.m.u.), $NaBH_4$ (96%, 37.83 a.m.u.), NH_4OH (28% in H2O, 35.05 a.m.u.) , Polyvinyl alcohol (87-89% hydrolyzed, 13-23 kDA), CTAB (99%, 364.45 a.m.u.), L-ascorbic acid (99%, 364.45 a.m.u.) were purchased from Sigma Aldrich. All the chemicals were used without any further purification.

2.2.2 Synthesis of Au/Ag NPs with the dilution of precursor

The 'in situ synthesis' of Au/Ag NPs were carried out by modification in classical wet chemistry method [24]. In a typical experiment, 33.80 mg of $HAuCl_4.3H_2O$ (99.99%, 393.83 a.m.u.) and 52.22 mg of $AgNO_3$ (99%, 169.87 a.m.u.) were added in 3 mL H_2O respectively to make stock solutions. Both metal precursor salts were weighed directly into a black microcentrifuge tube with Teflon coated spatula, to prevent wastage and contamination. Later, 3.01 mg of $NaBH_4$ (96%, 37.83 a.m.u.) and 250.48 mg of powdered Tri-sodium citrate dehydrate (294.10 a.m.u.) were mixed in 30 ml and 25 ml of H_2O and stored as stock solutions. Ten 50 mL test tubes labeled Au 25, Au 20, Au 15 Au 10, Au 5, Ag 25 Ag 20, Ag 15, Ag 10 and Ag 5 followed by addition of 25 mL, 20 mL, 15 mL, 10 mL and 5 mL of H_2O according to the label respectively. Further, 443 µl of prepared $HAuCl_4.3H_2O$ solution was mixed for Au NPs and 126 µl of prepared $AgNO_3$ solution is mixed Ag NPs with 1 minute stirring at 300 rpm. 250 µl of Tri-sodium citrate dehydrate stock solution was added for Au NPs and Ag NPs respectively followed by addition of 1 mL of prepared $NaBH_4$ solution in each test tube. Nanoparticle formation was observed by the color change and colloidal solutions thus formed were left for 5 min stirring at 300 rpm and stored in the freezer.

2.2.3 Synthesis of Au/Ag NPs with a varying citrate concentration

Au/Ag NPs were synthesized with different concentrations of citrates. In a typical experiment, 15.60 mg of $HAuCl_4.3H_2O$ (99.99%, 393.83 a.m.u.) and 30.10 mg of $AgNO_3$ (99%, 169.87 a.m.u.) were added in 1.5 mL H_2O respectively to make stock solutions. Both metal precursor salts were weighed directly into a black microcentrifuge tube with Teflon coated spatula. Later, 3.01 mg of $NaBH_4$ (96%, 37.83 a.m.u.) and 200.51 mg of powdered Tri-sodium citrate dehydrate (294.10 a.m.u.) was mixed in 30 mL and 5 mL H_2O respectively and stored as stock solutions. 25 mL H2O were taken into ten test tubes labeled Au 25, Au 25*2, Au 25*4, Au 25*8, Au 25*16, Ag 25, Ag 25*2, Ag 25*4, Ag 25*8, Ag 25*16 respectively. 443 µl of prepared $HAuCl_4.3H_2O$ solution was mixed for Au NPs and 126 µl of prepared $AgNO_3$ solution is mixed for Ag NPs with 1 minute of stirring at 300 rpm. 63 µl, 125 µl, 250 µl, 500 µl, 250 µl of Tri-sodium citrate dehydrate stock solution was added followed by addition of 1 mL of prepared $NaBH_4$ stock solution in each test tube. Nanoparticle formation was observed in 5 seconds by color change wine red for Au NPs and greenish yellow for Ag NPs. Solutions were left for 5 min of stirring at 300 rpm and stored in the freezer.

2.2.4 Synthesis of different aspect ratio Gold nanorods

Au NRs of different sizes and aspect ratio were synthesized by varying $AgNO_3$ concentration. In a typical experiment, 39.38 mg of $HAuCl_4.3H2O$ (99.99%, 393.83 a.m.u.) and 8.49 mg of $AgNO_3$ (99%, 169.87 a.m.u.) was added in 10 mL and 5 mL of DI water to make 10 mM stock solutions. Both metal precursor salts were weighed directly into a black microcentrifuge tube with Teflon coated spatula, to prevent wastage and contamination. Later, 3.01 mg of $NaBH_4$ (96%, 37.83 a.m.u.) and 88.06 mg of ascorbic acid (176.12 g/mol) were added separately in 5 mL H_2O to make 10 mM and 100 mM of stock solutions respectively. 5.468 g of CTAB (364.45 g/mol) in 150 mL DI water was prepared which acts as a surfactant. 10 mL of freshly prepared CTAB was taken into a 15 mL test tube and labeled as Au seed. Later, 250 µl of prepared $HAuCl_4.3H_2O$ solution was mixed followed by the addition of 600 µl of prepared NaBH4 stock solution and left for 5 minutes stirring at 300 rpm. The solution was kept undisturbed for 1 hour to allow the gold seed formation. Once the Au seed is prepared, 10 mL of prepared CTAB were taken into five test tubes labeled Au NR 60, Au NR 80, Au NR 100, Au NR 120 and Au NR 150. Later, 500 µl of prepared $HAuCl_4.3H_2O$ was added followed by 60 µl, 80 µl,100 µl, 120 µl and 150 µl of $AgNO_3$ respectively. 200 µl of 1.2 M HCl was added to make the solution acidic. This was followed by the addition of 100 µl of L-ascorbic acid. Subsequently, 30 µl of prepared Au seed solution was added and kept in a water bath at 45° C for 30 minutes. Au NRs formation is observed due to the vibrant color change to blue, wine red to burgundy.

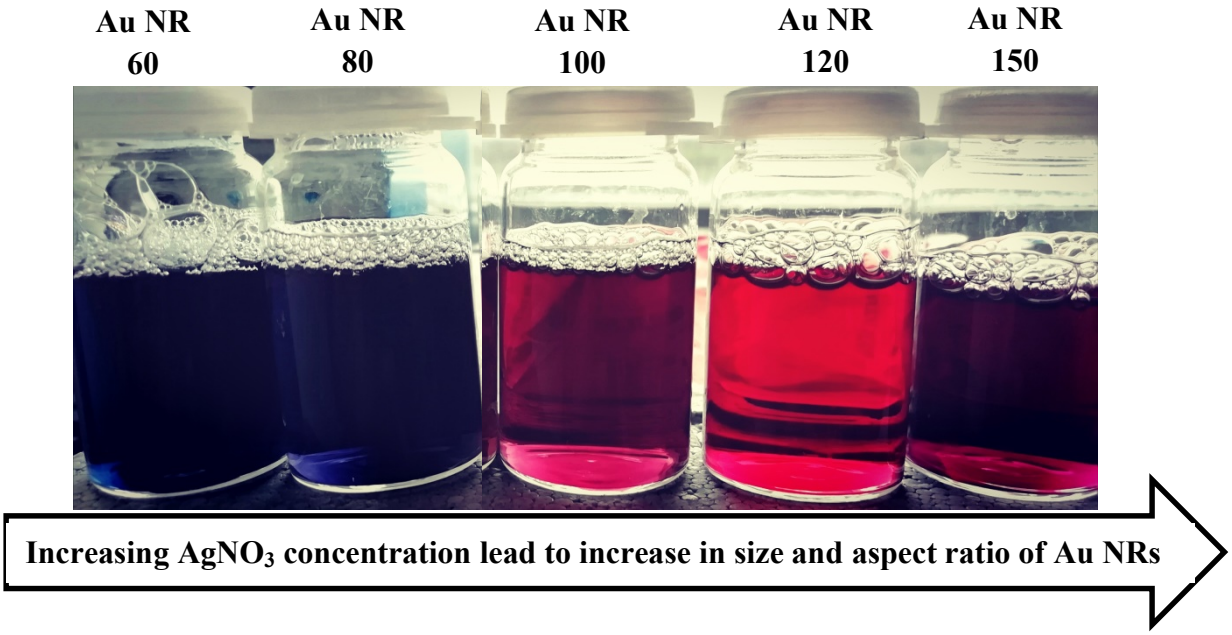

Fig. 2.2: Optical photograph showing the variation in the color of gold nanorods with a change in their size and aspect ratio on increasing concentration of $AgNO_3$.

2.2.5 Synthesis of the homogeneously alloyed nanoparticle of gold and silver in H20 and PVA.

Homogeneously alloyed bi-metallic NPs of gold and silver were synthesized in H20 and PVA solution separately [9]. In a typical experiment, 31.60 mg of powdered $HAuCl_4.3H_2O$ (99.99%, 393.83 a.m.u.) and 16.99 mg of powdered $AgNO_3$ (99%, 169.87 a.m.u.) were added in 4 mL H_2O respectively. Both metal precursor salts were weighed directly into a black microcentrifuge tube with Teflon coated spatula, to prevent wastage and contamination. Later, 2.05 mg of $NaBH_4$ (96%, 37.83 a.m.u.) and 202.31 mg of powdered Tri-sodium citrate dehydrate (294.10 a.m.u.) was mixed in 20 mL and 5 mL H_2O respectively and stored as stock solutions. Five 50 ml test tubes were filled with 15 ml H_20 and five 50 ml test tubes were filled with 15 ml of PVA solution respectively and labeled as shown in the figure below. 625 µl, 468 µl, 312 µl, 156 µl and 0 µl of prepared $AgNO_3$ solution were mixed in order followed by treatment with 80, 60, 40, 20 and 0 µl of NH_4OH (1 mol) respectively for both cases (H_2O and PVA). The total volume of each solution was made 25 ml by diluting with appropriate amount of H_2O/PVA and left for 2 minutes of stirring at 300 rpm for uniform mixing. Later, 250 µl of Na_3Ct (25 mmol) was added in each solution followed by addition of 0 µl, 156 µl, 312 µl, 468 µl and 625 µl of $HAuCl_4.3H_2O$ solution in the same order as mentioned above with 5 minutes of stirring at 500 rpm. 1 mL of prepared $NaBH_4$ stock solution was added in each test tube at last. Nanoparticle formation was observed in 5 seconds giving different colors to the solution depending on its size and molar ratio of gold and silver. Samples were stored in the freezer for 5 hours.

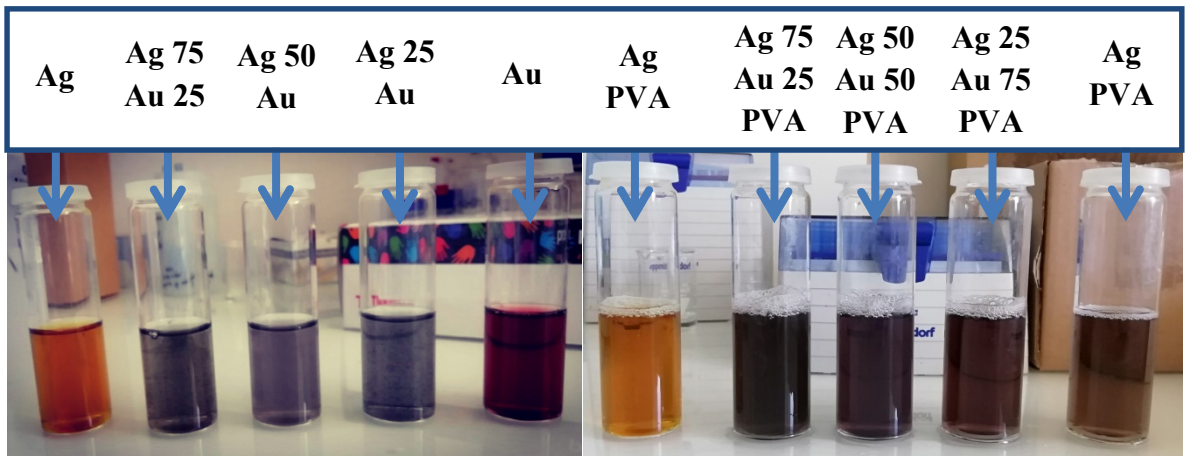

Fig. 2.3: Optical photograph showing the variation in the color of homogeneously alloyed Ag-Au NPs with the different molar ratio of metal precursor (a) in H_20 and (b) in PVA.

2.3 Characterization Techniques

2.3.1 Dynamic Light Scattering

The size of colloidal metal nanoparticles can be determined by measuring the random changes (Brownian motion) in the scattered light intensity from the suspension. The scattering intensity measured from DLS depends on the 6th power of the size and is used to derive other physical quantities like the hydrodynamic size and zeta potential [29]. Measurements of hydrodynamic size and zeta potential were made on a Malvern Zetasizer applying the dynamic light scattering method (DLS). The configuration was checked by Zetasizer software. All measurements were conducted at a temperature of 25 °C with equilibration time 120 sec for 1st reading and 0 sec for the later readings. All the colloidal suspension was diluted in proper solvents and the concentration of NaCl was kept at 10^{-2} M. Three repeated measurements were taken to investigate for result repeatability.

2.3.2 UV-Vis Spectroscopy

Gold and silver NPs show a special optical feature known as “localized surface plasmon resonance” (LSPR) which gives a strong absorption in the UV-vis region [23]. It is a very important tool to predict the shape and size and optical properties of NPs. All the colloidal suspension were characterized using a UV-vis Shimadzu spectrometer in the wavelength range from 300 to 900 nm, with a resolution of 0.5 nm. The absorption spectra were recorded for each nanostructure. They show the fine-tuning of SPR peaks from visible to Near IR region.

2.3.3 Transmission Electron Microscopy

TEM microscopy is the commonly used technique to study the shape, size, and dispersion of gold and silver nanostructures at the sub-nanometer range. 20 µL of samples were dropped cast on a 400 mesh carbon-coated Cu grid (TadpellaInc) and kept to dry protected from dust. TEM, STEM, HRTEM and SAED imaging was performed on TECNAI G2 20 TWIN at 200 Kv. Several pictures were taken for each chosen NP sample. The average diameter of at least 300 particles of each sample was measured from these TEM images using the “Image J” software and a histogram, which was plotted to show the size distribution of the particles.

SAED pattern of each nanostructure was analyzed using Digital Micrograph and the corresponding lattice plane was indexed and matched with the ICDD files of gold and silver.

Chapter 3

3.1 Results and Discussion

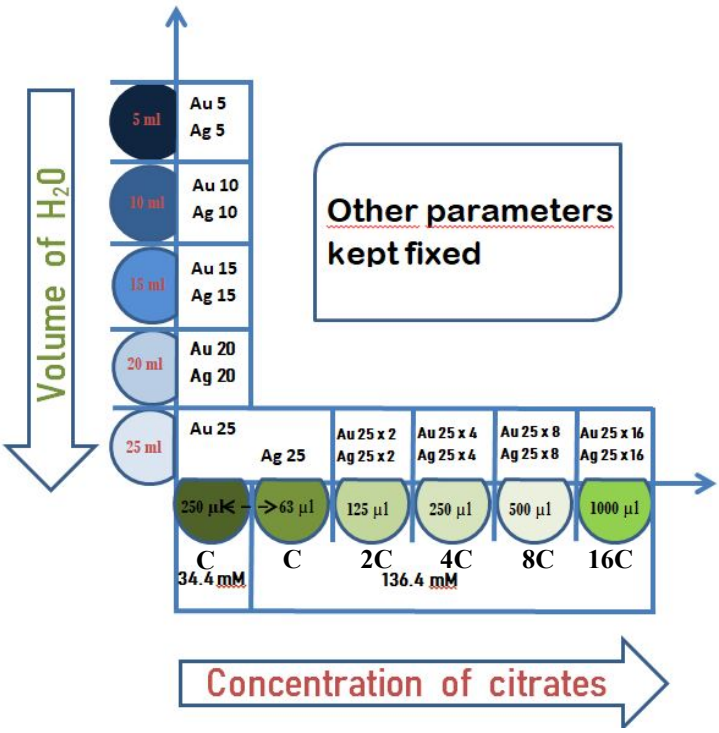

Fig. 3.1: Schematic of sample naming with the change in citrate concentration and precursor dilution. Different volumes of H20 and citrates were added to optimize NP synthesis and obtain uniform results

3.1.1 Role of the precursor dilution in the synthesis of gold and silver NPs

In order to develop the multifunctional nanoplatform and optimize the synthesis, we first checked the role of the metal precursor concentration in the synthesis of NPs [23], [24], [30]. We prepared five samples of Au and Ag NPs respectively with a dilution of metal precursor in H2O. The amount of H_2O added is varied while keeping all the other parameters fixed. The blend of dynamic light scattering, optical spectroscopy and electron microscopy is performed to investigate the shape, size and surface chemistry of the particles. We synthesized NPs having a varying core diameter. The hydrodynamic size (in number as well as in intensity)

and the polydispersity index were recorded by the DLS technique. Size in number gives information about NPs of small size, whereas size in intensity tells us about large NPs [29]. The results show the formation of NPs of different sizes (~10-50 nm) on the nanometer scale.

Table 3.1: Hydrodynamic size measurement of gold and silver NPs with metal precursor dilution

Sample	Hydrodynamic Size in number [d.nm] (average of 3)	Standard deviation (average of 3)	(PdI) (average of 3)	Hydrodynamic Size in Intensity [d.nm] (average of 3)	Standard deviation (average of 3)	(PdI) (average of 3)
Au 5	36	10	0.239	72	28	0.240
Au 10	37	11	0.233	78	31	0.236
Au 15	35	10	0.222	69	27	0.222
Au 20	35	10	0.239	72	29	0.239
Au 25	34	10	0.248	69	27	0.248
Ag 5	37	7	0.569	56	36	0.603
Ag 10	42	10	0.576	66	35	0.529
Ag 15	12	3	0.565	52	31	0.548
Ag 20	8	2	0.559	49	27	0.538
Ag 25	18	5	0.475	43	22	0.526

Furthermore, to predict the shape and size of the NPs and to study their optical properties, the samples were characterized by UV-vis spectroscopy. The absorption spectra were recorded and compared to investigate the variation with the precursor dilution. The study reveals a blue shift in the SPR peak with the dilution of precursor for both gold and silver NPs which is attributed to a decrease in particle size [31]. The position and bandwidth of the SPR peak give us information about the particle size and uniformity. The size effect can be observed as a red shift with an increase in particle size. This can be explained by the retardation effects of the light-matter interaction when particle size is comparable to the wavelength of light [18].

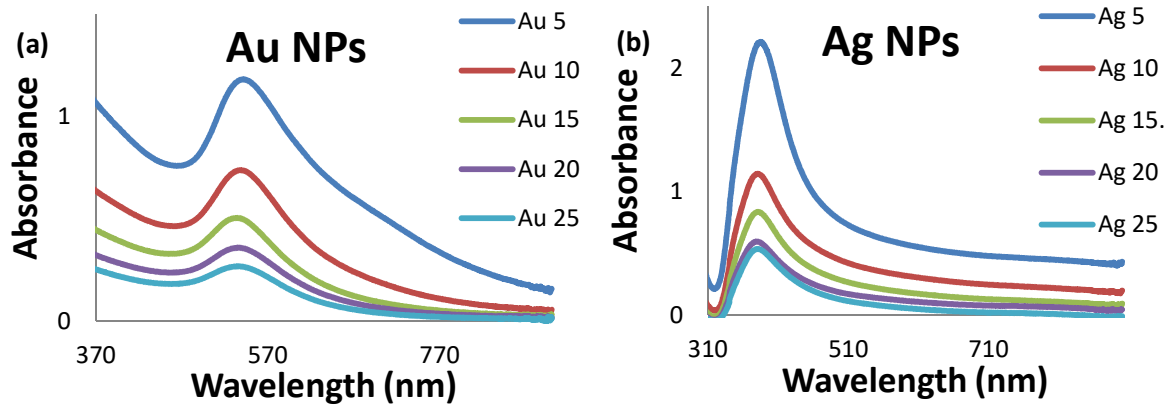

*Fig. 3.2: UV-vis spectra of **(a)** Au NPs and **(b)** Ag NPs showing a blue shift in SPR peak with metal precursor dilution. Blue shift in SPR peak refers to a decrease in particle size.*

With our overarching aim to find a pattern in the variation of size and morphology with the dilution of precursor, a detailed investigation was carried out using electron microscopy [31] [32]. Three samples of gold NPs and two samples of silver NPs namely Au 10, Au 20, Au 25,

Ag 10 and Ag 20 were chosen for TEM analysis. The results were studied for the structural, elemental and crystallographic analysis. The elemental composition is confirmed by the EDS analysis that shows an intense peak corresponding to gold and silver. The SAED pattern was indexed with corresponding lattice planes of gold.

Au 10: The sample named Au 10 has the highest metal precursor concentration and hence the capping of NPs is poor and can be seen from the uneven shape and size distribution. It can be alluded from TEM and STEM images that NPs of two different sizes are formed, some being as small as 4 nm(lighter) and some as large as 20 nm(darker). Big particles look darker, because of a large thickness that causes more diffraction of electrons falling on it.

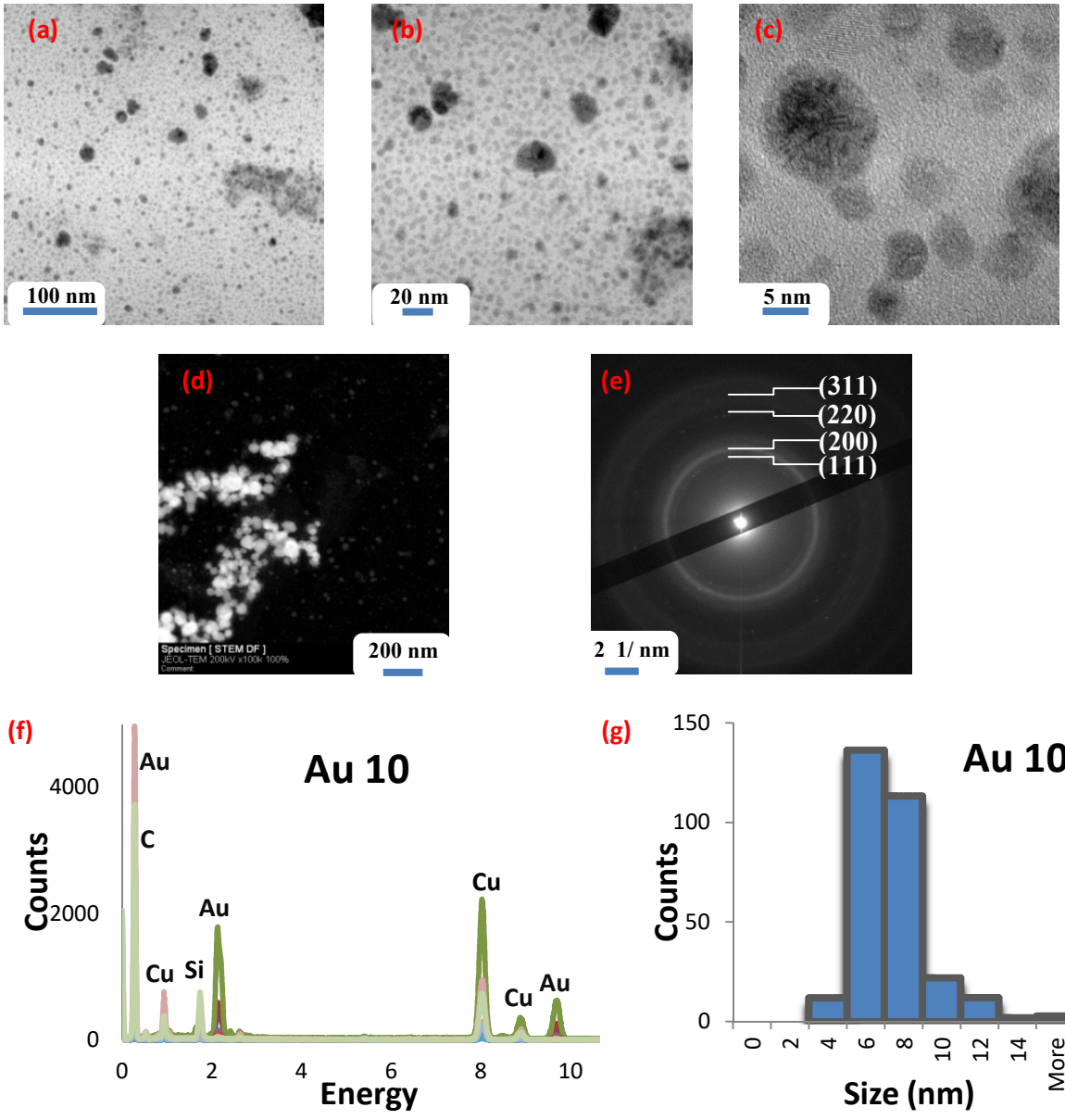

Fig.3.3: Representative TEM images of gold NPs with the highest metal precursor concentration at a scale length of ***(a)*** *100 nm,* ***(b)*** *20 nm,* ***(c)*** *5 nm,* ***(d)*** *STEM image (dark field) at a scale length of 200 nm showing NPs formation of two sizes,* ***(e)*** *SAED pattern indexed with corresponding lattice planes of gold,* ***(f)*** *EDS spectra showing intense peak for gold,* ***(g)*** *Histogram showing size distribution of 300 NPs with a bin size of 2 nm and an average particle diameter of* ***6.4 ± 2.6 nm****.*

Au 20: When the volume of H_2O is increased, a control on NPs shape and dispersity is observed. Dilution makes more room for NP synthesis and improves dispersion. TEM images show spherical particles uniformly dispersed. HRTEM and STEM images reveal the presence of NPs as small as 5 nm.

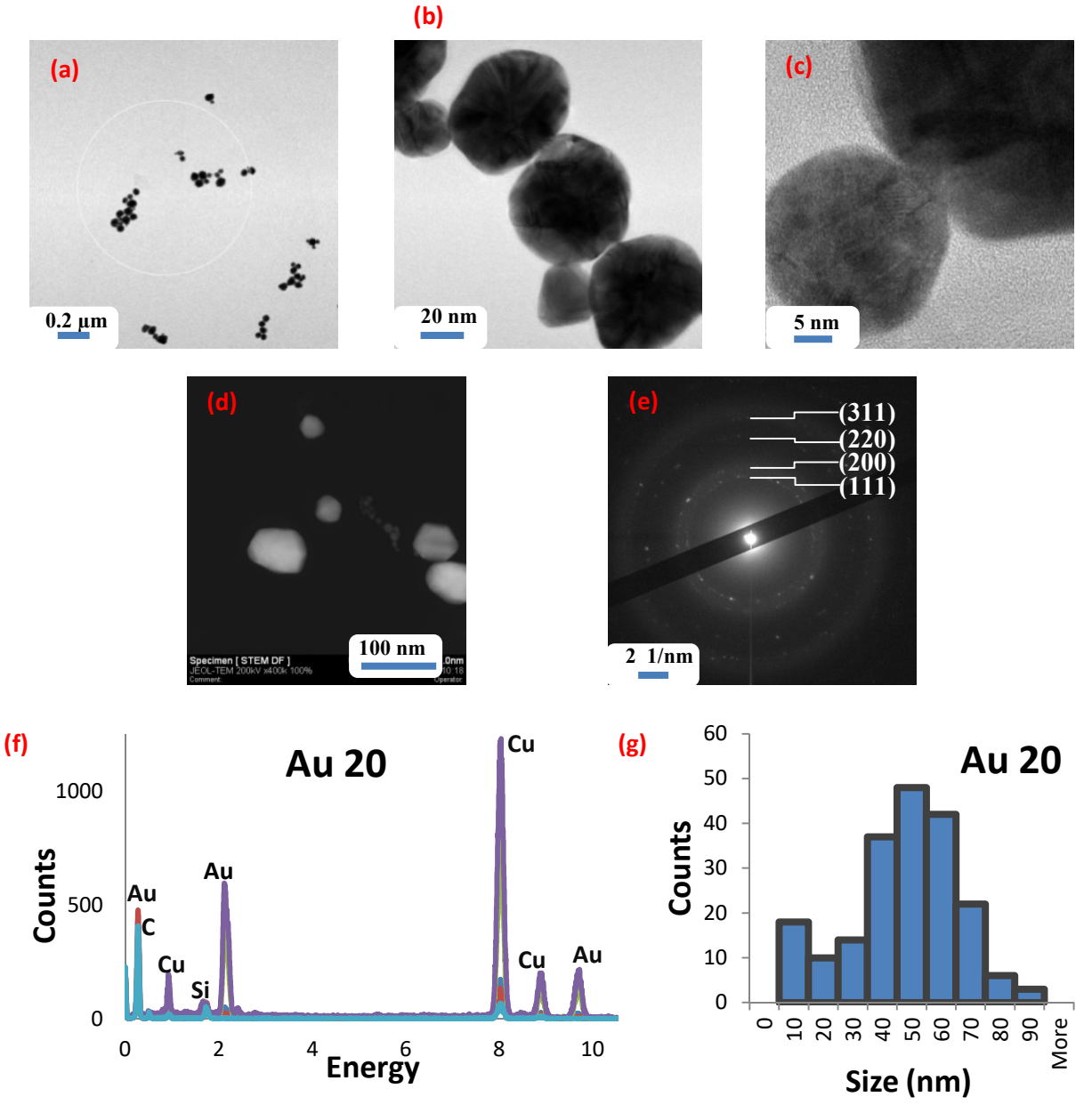

Fig.3.4: Representative TEM images of gold NPs with a dilution of metal precursor concentration at a scale length of ***(a)*** *0.2 µm,* ***(b)*** *20 nm,* ***(c)*** *5 nm,* ***(d)*** *STEM image (dark field) at a scale length of 100 nm showing NPs formation of two sizes,* ***(e)*** *SAED pattern indexed with corresponding lattice planes*

of gold, ***(f)*** *EDS spectra showing intense peak for gold,* ***(g)*** *Histogram showing size distribution of 300 NPs with a bin size of 10 nm and an average particle diameter of* ***42.3 ± 18.3 nm****.*

Au 25: With further dilution, both big and small NPs were observed with greater control on shape and size compared to previous results. The dilution plays a critical role in the further growth of NPs after nucleation. However, nano-sized lumps of gold have a tendency to grow bigger and to control the size a protective coating of molecules (like citrates) is necessary on the surfaces of the growing particles. Citrates prevent the increase in particle size and agglomeration. Au 25 sample shows good stability and uniform results. To get rid of large NPs (size more than 20 nm), concentration of citrates was planned to increased to prevent additional gold atoms to react and increase the particle size.

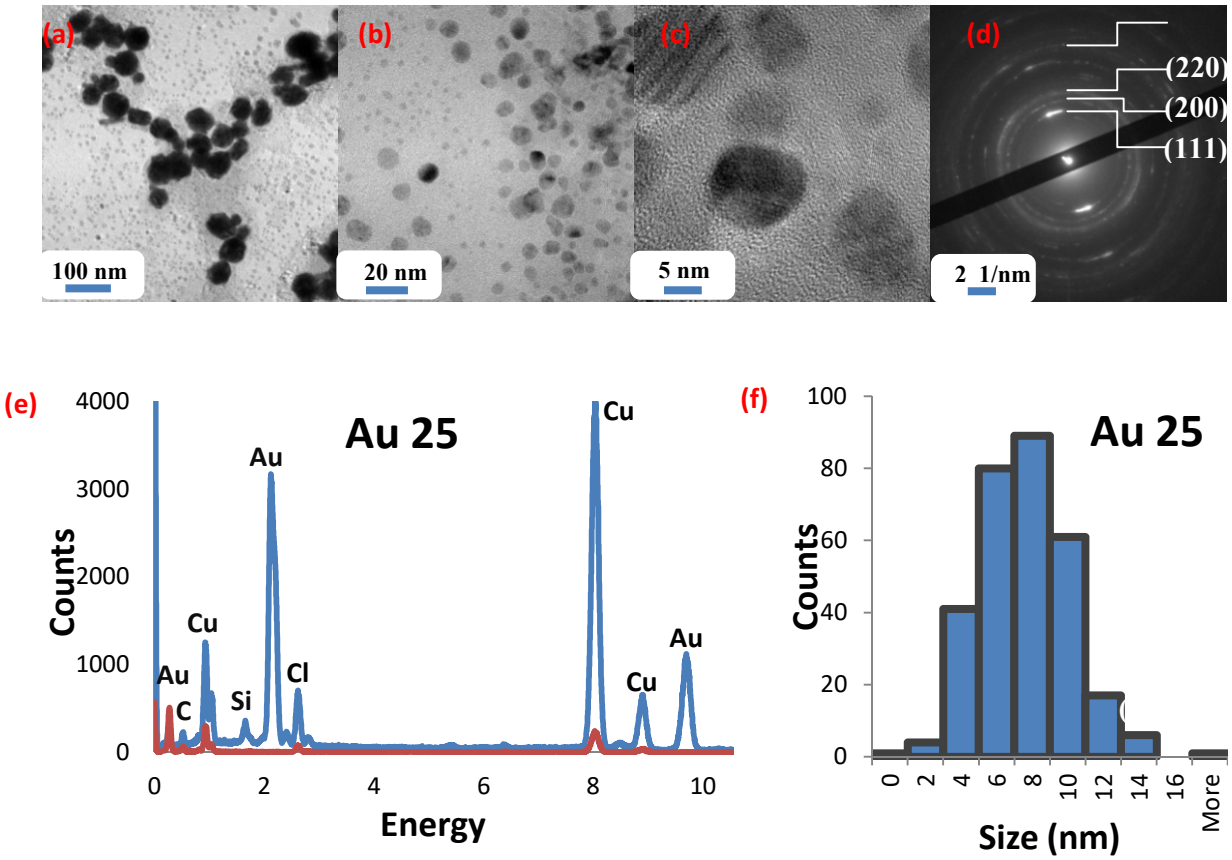

Fig.3.5: Representative TEM images of gold NPs at a maximum dilution of metal precursor concentration at a scale length of ***(a)*** *100 nm,* ***(b)*** *20 nm,* ***(c)*** *5 nm,* ***(d)*** *SAED pattern indexed with corresponding lattice planes of gold,* ***(e)*** *EDS spectra showing intense peak for gold,* ***(f)*** *Histogram*

showing size distribution of 300 NPs with a bin size of 2 nm and an average particle diameter of ***6.6 ± 2.6 nm****.*

Ag 10: Silver nanoparticles with the highest metal precursor concentration show huge agglomeration and coalescence with a wide distribution of the shape and size distribution. HRTEM and STEM reveal the presence of NPs as small as 2 nm. In STEM mode, the contrast depends on the thickness and the atomic number of particles. Hence, by increasing the contrast smaller particles are more visible and bigger ones appear blurred.

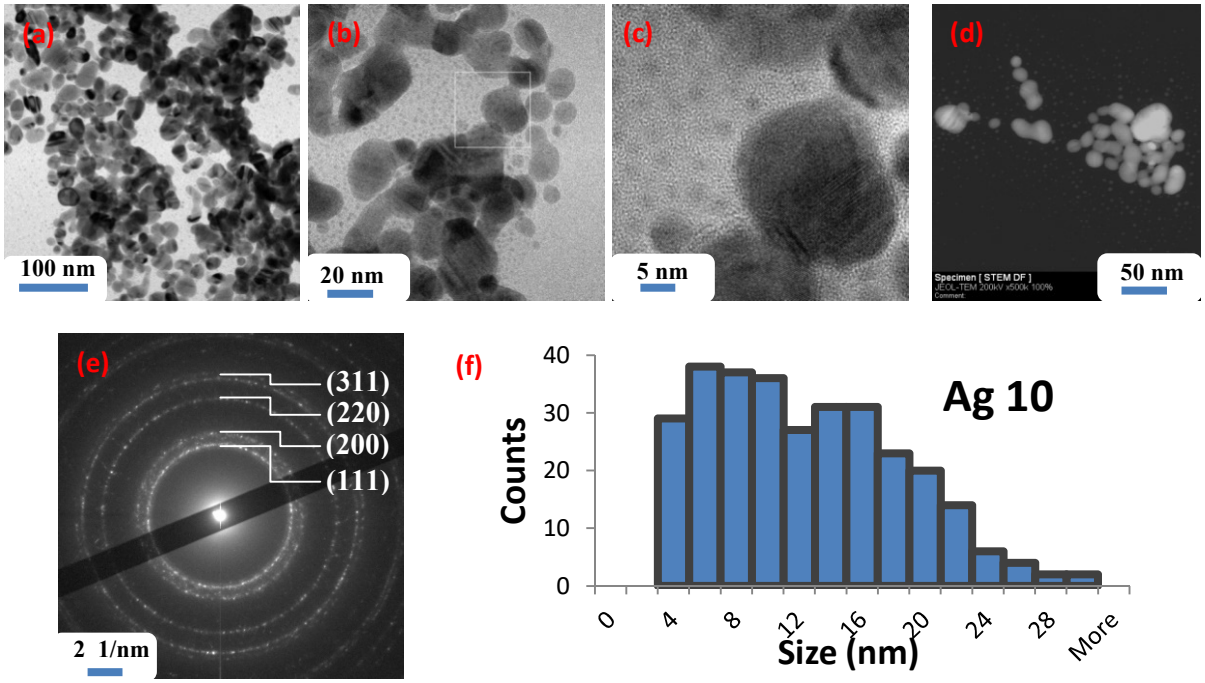

Fig.3.6: Representative TEM images of silver NPs with the highest metal precursor concentration at a scale length of ***(a)*** *100 nm,* ***(b)*** *20 nm,* ***(c)*** *5 nm,* ***(d)*** *STEM image (dark field) at a scale length of 50 nm showing NPs formation of two sizes,* ***(e)*** *SAED pattern indexed with corresponding lattice planes of gold,* ***(f)*** *Histogram showing size distribution of 300 NPs with a bin size of 2 nm and an average particle diameter of* ***11.5 ± 6.0 nm.***

Ag 20: The dispersity of silver NPs improved upon dilution with uniform size distribution. Agglomeration of particle reduced greatly with a uniform dispersion. The SAED pattern indexed with corresponding lattice planes confirms the presence of silver when matched with the ICDD file of silver. However, coalescence of NPs was still persistent. The sample was

kept under heavy e beam exposure for 15 minutes which could have been a cause for the coalescence of NPs, but no significant change was observed. If the coalescence is happening after a few seconds after beam exposure, it becomes very hard to detect.

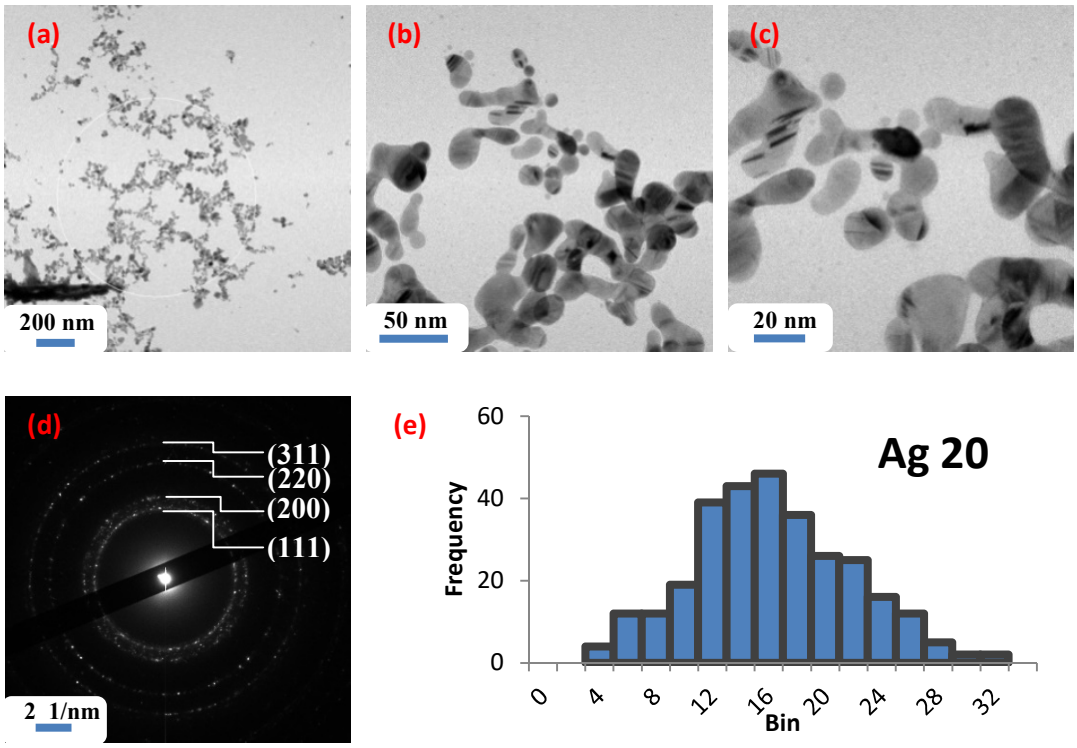

Fig.3.7: Representative TEM images of silver NPs with a dilution of metal precursor concentration at a scale length of ***(a)*** *200 nm,* ***(b)*** *50 nm,* ***(c)*** *20 nm* ***(d)*** *SAED pattern indexed with corresponding lattice planes of silver,* ***(e)*** *Histogram showing size distribution of 300 NPs with a bin size of 2 nm and an average particle diameter of* ***15.2 ± 5.5 nm****.*

Conclusion

DLS data for hydrodynamic size suggest that we prepared Au/Ag NPs of size ranging 10-60 nm for prepared with different dilution of metal precursor. UV-vis data shows a blue shift with dilution of precursor which suggests a decrease in particle size. The shape and size of NPs were confirmed from the electron microscopy. TEM images show the formation of NPs of two different sizes. The SAED pattern obtained by electron diffraction from the region of interest were indexed to the corresponding lattice planes and compared with the ICDD files of gold and silver which show great correlation.

The increase in particle size and uneven shape can be due to insufficient amount of stabilizing agent with an increasing metal precursor concentration [33]. The amount of citrate ions available to stabilize the particles was kept fixed and there simply would not be enough

to stabilize all the particles for high metal precursor concentration. This leads to the agglomeration into bigger particles until the total surface area turns out to be small enough to be capped by the citrate ions.

3.1.2 Influence of the concentration of citrates in the synthesis of gold and silver NPs.

Our aim for the next experiment was to change one parameter *i.e.* the citrate concentration while keeping all the other parameters fixed [34]. Citrates control the crystallite size and the oxidation degree of the metallic ions. They act as a capping agent and hence prevent the agglomeration of gold NPs. The size of the NPs highly depends on how effectively it is capped. It is also possible to modify the order of addition of citrate and $NaBH_4$ solution during synthesis in order to get different results [6]. We planed to add $NaBH_4$ at last. This allowed citrate molecules in reducing and capping of gold ions [35]. We prepared 5 samples using different concentrations of the citrate solution for gold and silver NPs respectively. The citrate concentration is increased by 2, 4, 8 and 16 times compared to the previous trial of Au25/Ag 25. The samples prepared with different citrate concentrations were pre-analyzed via basic characterization techniques like DLS and UV-vis spectroscopy. The DLS results suggest NP formation of a smaller core diameter and uniform results than previous trials. Size in number was taken into consideration as it tells about the majority of the particles.

Table 3.2: Hydrodynamic size measurement of gold and silver NPs showing decrease in size with increasing concentration of citrates. Small PdI means the NPs are uniformly dispersed. Negative zeta potential tells that NPs are capped by citrate molecules.

Sample	Hydrodynamic Size in number [d.nm] (average of 3)	Standard deviation (average of 3)	(PdI) (average of 3)	Zeta Potential [mV] (average of 3)	Standard deviation (average of 3)
Au 25	47	12	0.384	-11.1	8.77
Au 25*2	12	3	0.533	-12.5	9.12
Au 25*4	18	5	0.353	-22.5	11.73
Au 25*8	16	4	0.395	-26.6	11.40
Au 25*16	20	5	0.318	-22.1	9.94
Ag 25	23	6	0.340	-11.3	9.80
Ag 25*2	18	5	0.501	-13.3	11.45
Ag 25*4	26	7	0.397	-19.7	8.61
Ag 25*8	18	5	0.490	-15.6	12.33
Ag 25*16	19	5	0.408	-9.9	7.67

In order to have a better look into the variation in size, morphology and dispersion of NPs with increasing citrate concentration, the absorption spectra were studied and compared. The UV-vis results show a small red shift for Ag NPs suggesting a little increase in particle size

and a significant blue shift for Au NPs which is attributed to a decrease in particle size with increasing concentration of citrate. The samples were kept at 0° C for a couple of weeks to check the stability of colloids. The gold NPs with the least citrate concentration became heterogeneous with thick lumps in several months. In contrast, Ag NPs were stable.

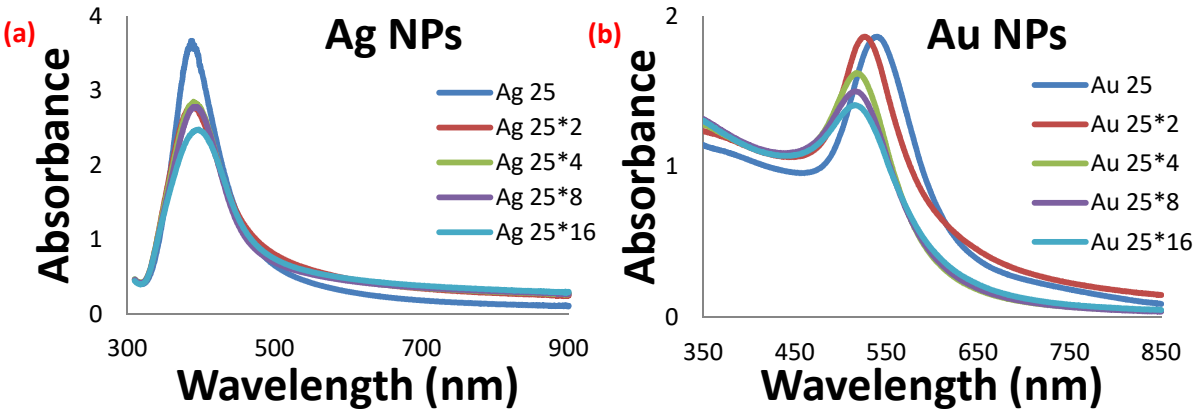

*Fig. 3.8: UV-vis spectra of **(a)** Ag NPs showing little blue shift in SPR peak and **(b)** Au NPs showing a significant blue shift in SPR peak with increasing citrate concentration.*

We aim to check the influence of the citrate concentration on the Au NPs dispersion and morphology via TEM. Three samples of gold NPs and one sample of silver NP namely Au 25*2, Au 25*4, Au 25*16 and Ag 25*4 were analyzed. We observed the NPs under different magnification to study the size distribution, morphology, and dispersion. HRTEM was used to see the array of gold atoms and a crystallographic analysis was performed to confirm the presence of gold and silver. However, the coalescence of the NPs can be observed when the magnification is more than 400K. This can be explained as due to decomposition of organic layer by beam exposure. We interest to look at the size distribution and the dispersion of NPs at the scale of 100 nm.

Au 25*2: The sample named Au 25*2 has the citrate concentration twice as compared to Au 25 which produces majority of small spherical NPs having similar sizes (< 20 nm). However, it can be seen from the TEM images that few NPs with a large core diameter (as large as 50 nm) were formed again. Capping is essential to control the shape, size and uniform dispersion i.e. The larger the concentration of citrate the more uniform the NPs are.

(a)

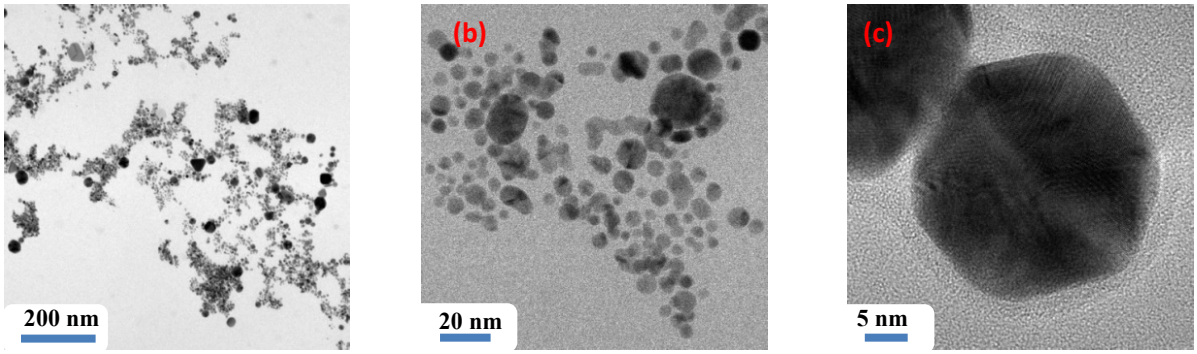

Fig. 3.9: Representative TEM images of gold NPs with the concentration of citrates increased two times at a scale length of ***(a)*** *200 nm,* ***(b)*** *20 nm,* ***(c)*** *5 nm.*

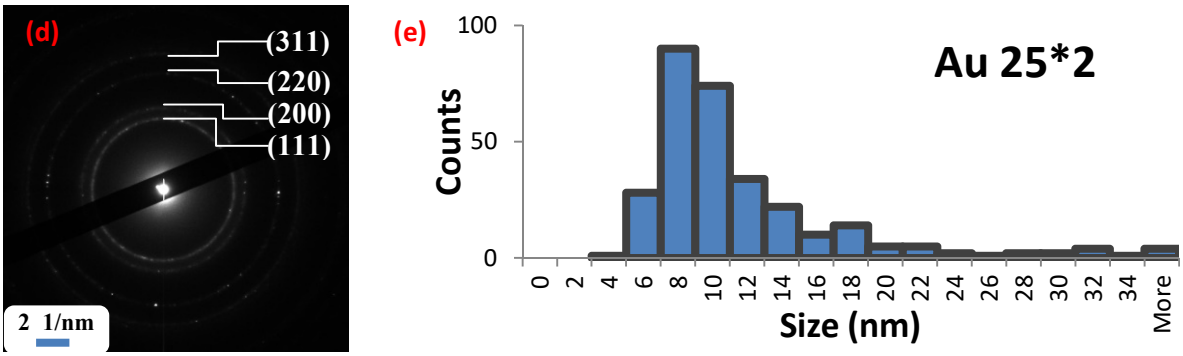

Fig. 3.9: ***(d)*** *SAED pattern indexed with corresponding lattice planes of gold,* ***(e)*** *Histogram showing size distribution of 300 NPs with a bin size of 2 nm and an average particle diameter of* ***10.6 ± 6.3 nm****.*

Au 25*4: When the concentration of citrate is increased four times, the NPs are more spherical and uniformly dispersed in the range of 3-7 nm. This shows that the citrate concentration is a crucial parameter for the growth and dispersion of the gold NPs. The decrease of the size of the gold NPs with increasing citrate concentration is compatible with the TEM results and the blue shift in the UV-vis peak.

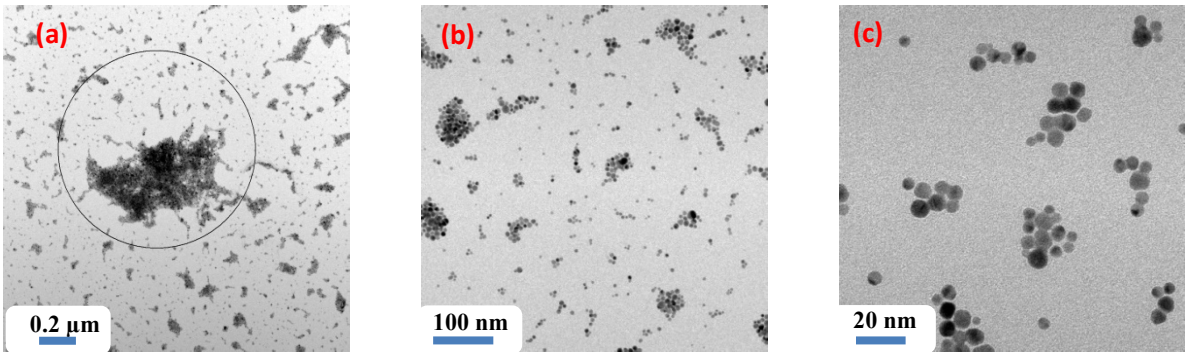

(e)

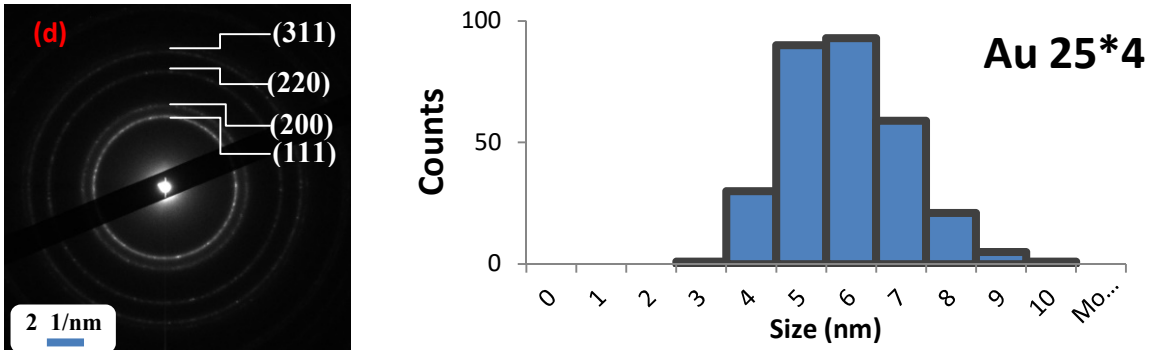

Fig. 3.10: Representative TEM images of gold NPs with concentration of citrates increased four times at a scale length of ***(a)*** *0.2 µm,* ***(b)*** *50 nm,* ***(c)*** *20 nm* ***(d)*** *SAED pattern indexed with corresponding lattice planes of gold,* ***(e)*** *Histogram showing size distribution of 300 NPs with a bin size of 1 nm and an average particle diameter of* ***5.4 ± 1.2 nm****.*

Au 25*16: For the sample with the highest citrate concentration, the dispersion is more uniform and the size of the NPs is in the 2-10 nm range. The number density is larger and the yield is greater.

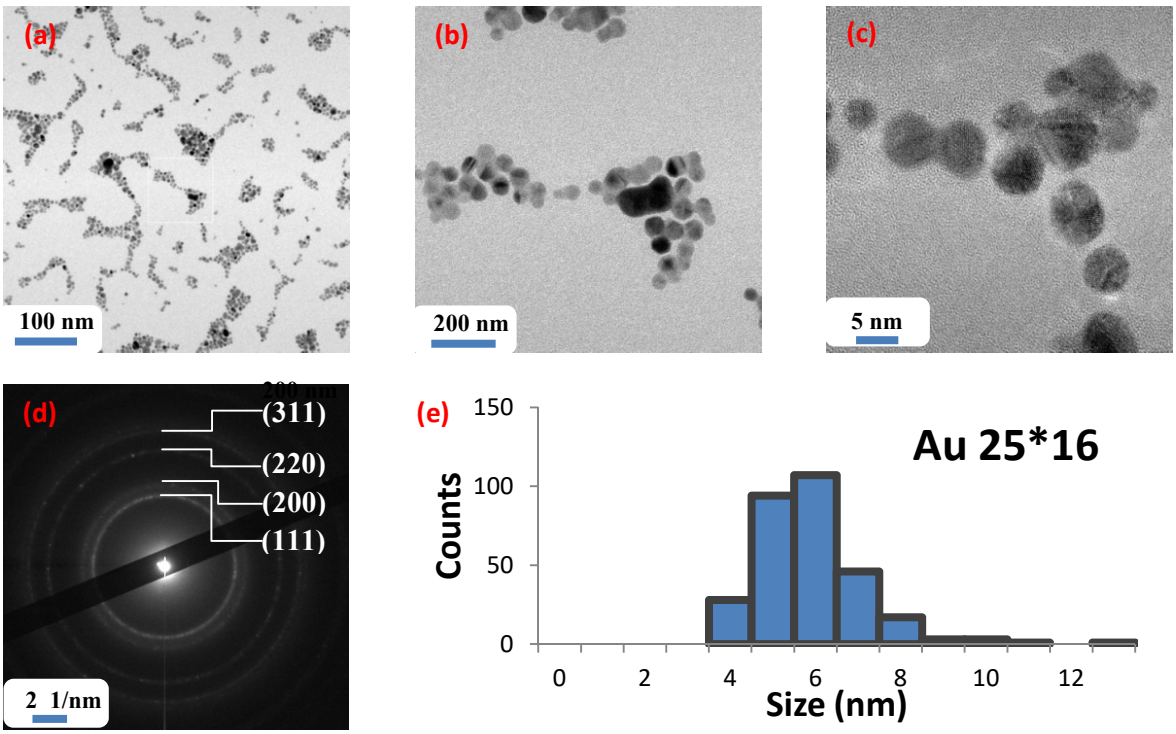

Fig. 3.11: Representative TEM images of gold NPs with concentration of citrates increased 16 times at a scale length of ***(a)*** *100 nm,* ***(b)*** *20 nm,* ***(c)*** *5 nm* ***(d)*** *SAED pattern indexed with corresponding lattice planes of gold,* ***(e)*** *Histogram showing size distribution of 300 NPs with a bin size of 1 nm and an average particle diameter of* ***5.4 ± 1.3 nm****.*

Ag 25*16: With increased dilution and the citrate concentration, NPs with particle size under 15 nm can be synthesized. Coalescence still remains the issue but uniformity in shape is achieved. The SAED pattern analysis provided us with information about the lattice planes which match with the ICDD data of silver.

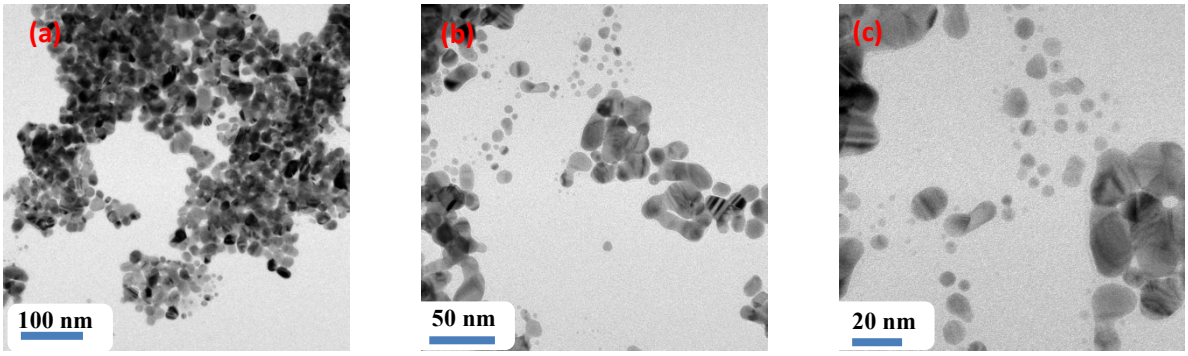

Fig. 3.12: Representative TEM images of silver NPs with the concentration of citrates increased 16 times at a scale length of ***(a)*** *100 nm,* ***(b)*** *20 nm,* ***(c)*** *5 nm*

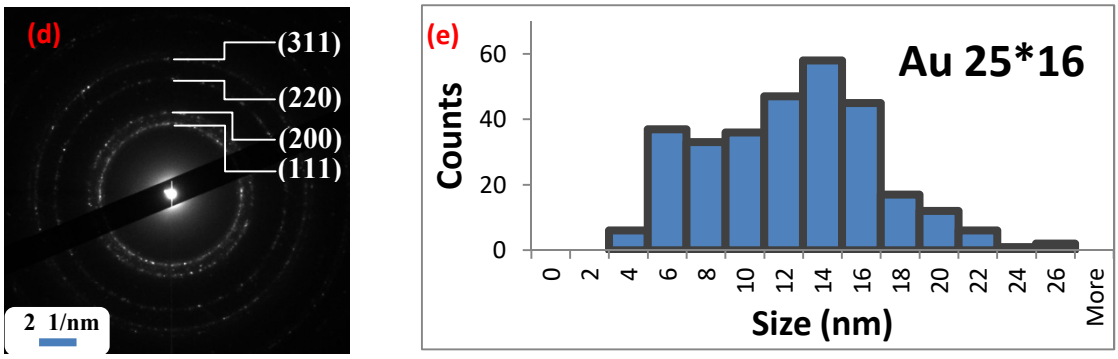

Fig. 3.12: ***(d)*** *SAED pattern indexed with corresponding lattice planes of silver,* ***(e)*** *Histogram with size distribution of 300 NPs with a 2 nm bin size and an average particle diameter of* ***11.4 ± 4.4 nm****.*

Conclusion

DLS data for hydrodynamic size suggest that we prepared Au/Ag NPs of size ranging from 10-50 nm using different concentrations of citrate solution. UV-vis data shows a small red shift for Ag suggesting an increase in particle size and blue shift for Au NPs suggesting a decrease in particle size with increasing concentration of citrates. The shape and size of NPs were confirmed from the electron microscopy. TEM images show the formation of NPs most of which fall in quantum confinement regime (particle size less than 15 nm) [36]. The SAED pattern obtained by electron diffraction from the region of interest were indexed to the corresponding lattice planes and compared with the ICDD files of gold and silver.

Table 3.3: Comparison of interplanar distance between lattice planes for gold and silver NPs with ICDD files and indexing corresponding lattice planes.

3.1.3 Introducing structural anisotropy and plasmon band in NIR region with the formation of gold nanorods in CTAB.

Gold nanorods with two different aspect ratios were synthesized by seed-mediated growth tuning optical response to the NIR region [37]. Biological tissues are relatively transparent to near-infrared radiation. The geometry of nanorods depends on several parameters like pH, the concentration of gold and silver precursor, the surfactant and temperature. Nanospheres are generally more stable and easy to synthesize which provides an SPR peak in the visible region. However, an intense peak in the NIR region for gold NRs makes them a good candidate for photothermal therapy and bio-medical applications [38]. With increased $AgNO_3$ concentration, Au seeds are covered more efficiently with Ag^+ leading to nanorod formation. Ag^+ ions form a monolayer in a special fashion inhibiting the growth in a particular direction [27]. The absence of $AgNO_3$ leads to the formation of bigger nanospheres.

(hkl)	Ag ICDD (Å)	Ag 10 (Å)	Ag 20 (Å)	Ag 25*4 (Å)	Au ICDD (Å)	Au 10 (Å)	Au 20 (Å)	Au 25 (Å)	Au 25*2 (Å)	Au 25*4 (Å)	Au 25*16 (Å)	Au NR 150 (Å)
(111)	2.35888	2.33889	2.35888	2.3417	2.355	2.35500	2.35500	2.3577	2.3587	2.34987	2.34018	2.3355
(200)	2.04285	2.01471	2.04285	2.04444	2.039	2.03900	2.03900	2.0325	2.04072	2.0325	2.028	2.04471
(220)	1.44451	1.431	1.44451	1.4423	1.442	1.44200	1.44200	1.44186	1.4375	1.43509	1.44209	1.2382
(311)	1.23188	1.21628	1.23188	1.2311	1.1774	1.17740	1.17740	1.1576	1.2295	1.22536	1.22409	
(222)	1.17944		1.17944		1.0196	1.01960	1.01960					
(400)	1.02143		1.02143		0.9358	0.93580	0.93580					0.9212
(331)	0.93732		0.93732		0.912	0.91200	0.91200					
(420)	0.91359		0.91359		0.8325	0.83250	0.83250					
(422)	0.8339		0.83399									

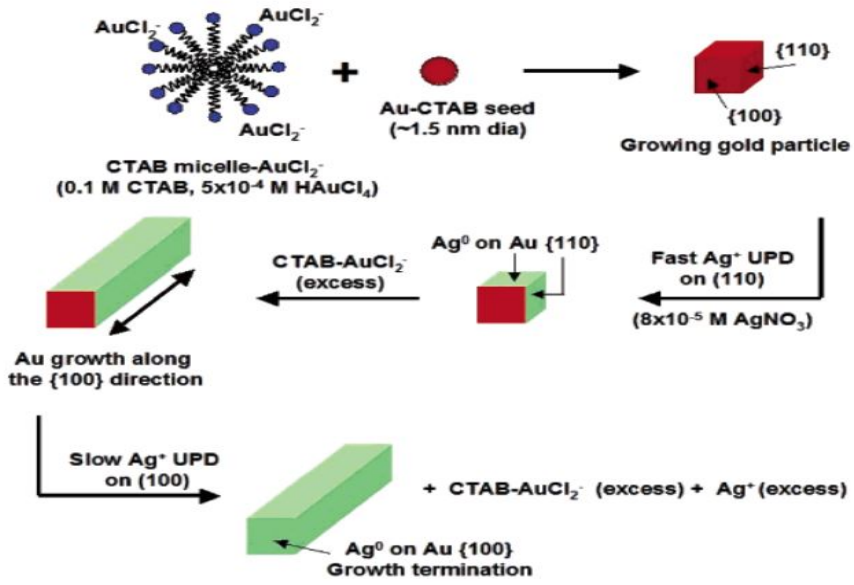

C. J. Murphy et al. J. Phys. Chem.B 2006, 110, 3990-3994

Fig. 3.13: Schematic of gold nanorod formation from CTAB capped Au seeds and role of Ag^+ in their growth. Ag+ ions form a monolayer in a special fashion inhibiting growth in a particular direction.

The presence of CTAB as a surfactant is crucial for the formation of nanorods. The first color change was observed for $HAuCl_4$ (light yellow). When $HAuCl_4$ was mixed with CTAB it gave a dark yellow color. This color change is attributed to Au-CTAB complex formation The yield of nanorods can be increased by increasing the CTAB concentration [39]. The addition of HCl increases the rate of dissociation of ascorbic acid which reduces Au(III)-CTAB complex to Au(I)-CTAB complex which is colorless.

UV-vis spectra show two absorbance peaks, one at ~520 nm in the visible region and the other at 700-1200 nm in the NIR region. These peaks are attributed to transverse and longitudinal SPR of Au NRs respectively. Longitudinal plasmon resonance peak in NIR region can be finely tuned because it is very sensitive to the aspect ratio of gold NRs [37].

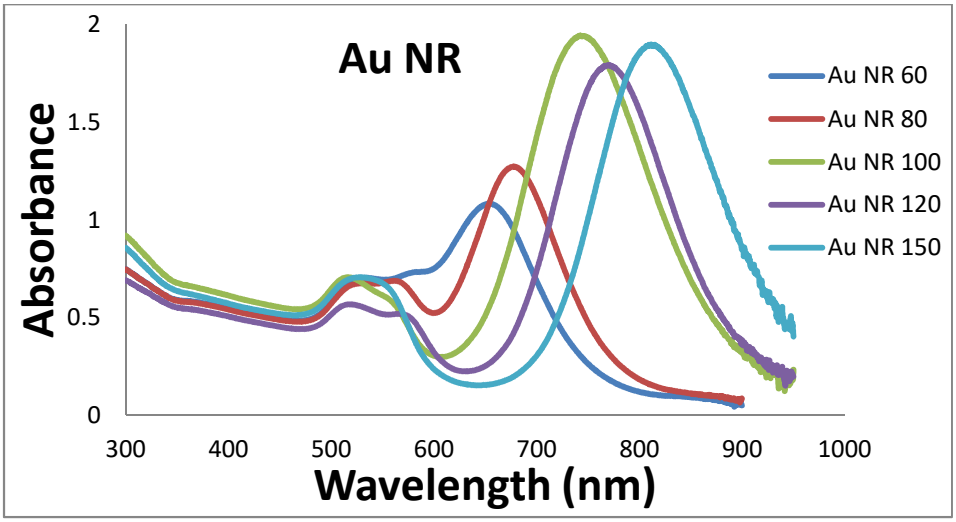

Fig. 3.14: UV-vis spectra of gold nanorods showing red shift in longitudinal SPR peak with increasing concentration of AgNO3 suggesting the formation of increased aspect ratio nanorods..

Two samples named Au NR 80 and Au NR 150 were taken in order to visualize the effect of $AgNO_3$ concentration on the shape, size, aspect ratio and dispersion. $AgNO_3$ concentration affects the growth of nanorods their size and aspect ratio can be increased by increasing $AgNO_3$ concentration.

Au NR 80: The sample Au NR 80**,** synthesized with 80 µl of $AgNO_3$, shows the formation of nanorods of small length and aspect ratio with fine control on dispersion. Some nanospheres were produced because of the low concentration of $AgNO_3$.

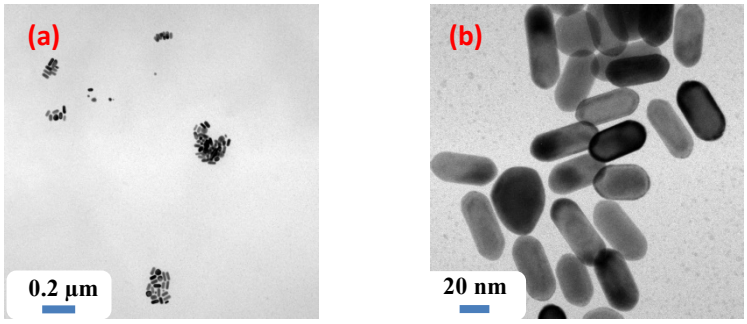

Fig. 3.15: Representative TEM images of gold nanorods synthesized with 80 µl of $AgNO_3$ at a scale length of ***(a)*** *0.2 µm,* ***(b)*** *20 nm. Synthesized nanorods were of small size and some nanospheres were obtained because of the low concentration of Ag^+* ions.

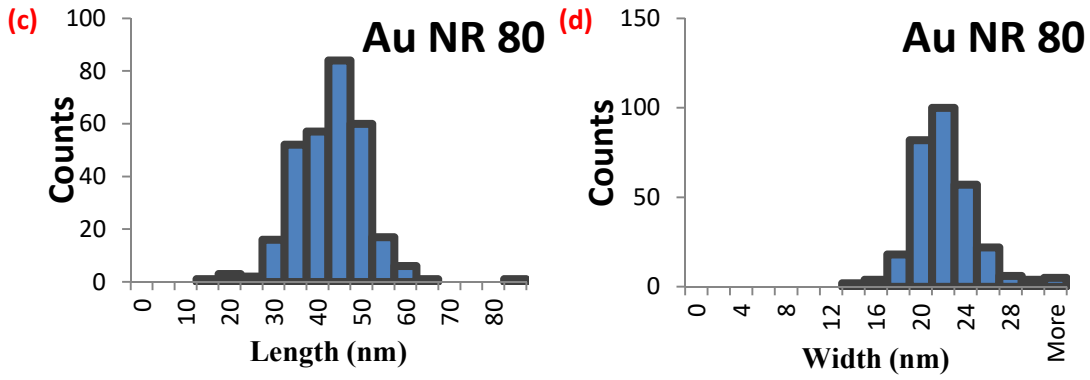

Fig. 3.15: ***(c)*** *Histogram showing length distribution of 300 NPs with a bin size of 5 nm and an average length of* ***40.6 ± 9.0 nm****.* ***(d)*** *Histogram showing width distribution of 300 NPs with a bin size of 2 nm and an average width of* ***21.3 ± 3.1 nm****.*

Au NR 150: The sample Au NR 150**,** synthesized with 150 µl of $AgNO_3$, shows the formation of long nanorods with increased aspect ratio and a fine control on dispersion. This can be attributed to an increased concentration of $AgNO_3$ which is a crucial parameter for nanorod synthesis.

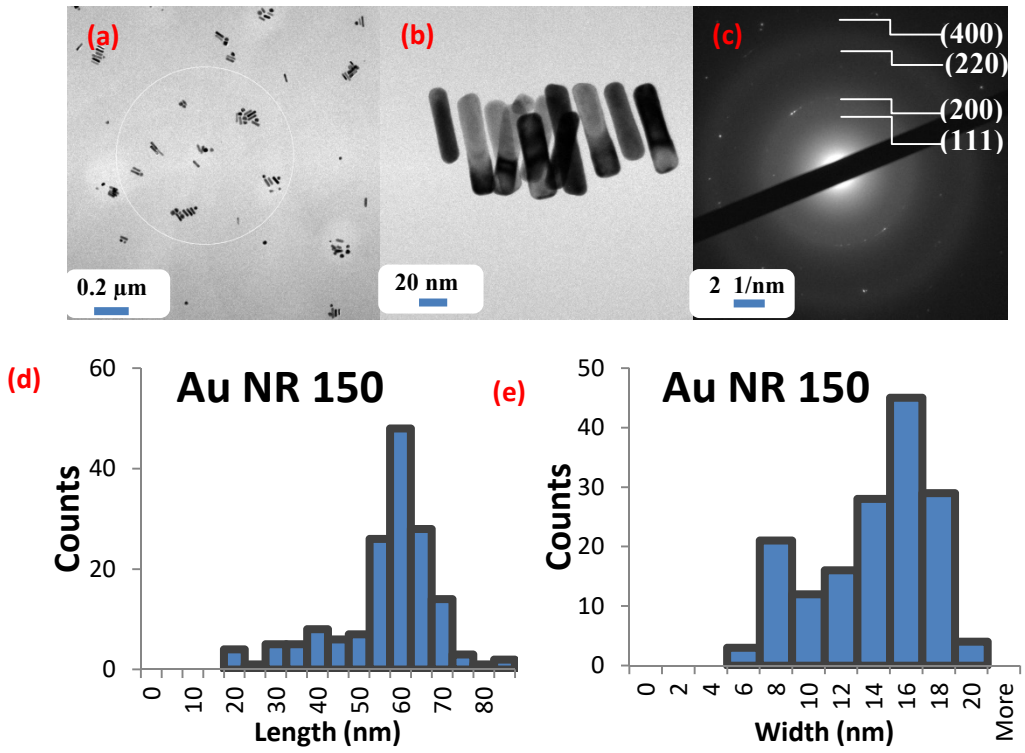

Fig. 3.16: Representative TEM images of gold nanorods synthesized with 150 µl of $AgNO_3$ at a scale length of ***(a)*** *0.2 µm,* ***(b)*** *20 nm,* ***(c)*** *SAED pattern indexed with corresponding lattice planes of gold.* ***(d)*** *Histogram showing length distribution of 160 NPs with a bin size of 5 nm and an average length of* ***54.2 ± 12.5 nm****.* ***(e)*** *Histogram showing width distribution of 160 NPs with a bin size of 2 nm and an average width of* ***13.0 ± 3.5 nm****.*

Conclusion

In order to obtain the SPR peak in NIR region, gold nanorods of different size and aspect ratio were synthesized by varying concentration of $AgNO_3$ using seed-mediated growth. UV-vis spectra show a significant red shift with the increase in $AgNO_3$ concentration, confirming an increase in size and aspect ratio of Au NRs. TEM analysis clearly reveals the formation of NRs whose size and SPR peak can be tuned by increasing the concentration of $AgNO_3$ which inhibits the growth in a special manner and crucial for the formation of Au NRs. Some other parameters like a mild reducing agent in the growth solution and CTAB as a surfactant are responsible for the formation of Au NRs.

Table 3.4: Aspect ratio calculated from mean length and width of gold nanorods with varying concentration of $AgNO_3$

Sample Name	Vol. of $AgNO_3$ (µL)	Mean length (nm)	Mean width (nm)	Mean Aspect Ratio
Au NR 80	***80***	***40.6 ± 9.0***	***21.3 ± 3.1***	***1.9***
Au NR 150	***150***	***54.2 ± 12.5***	***13.0 ± 3.5***	***4.2***

3.1.4 Tailoring optical property by controlled homogenous alloying of gold and silver NPs in H2O and PVA

The colloidal suspensions of Ag-Au alloy NPs in H_2O were stable after synthesis but precipitated in few days because of agglomeration of NPs except Ag 25 Au 75 which shows good stability and intermediate color between pure Ag NP and Au NP suggesting the formation of alloy NPs [40]. The hydrodynamic size (in number) and PdI were recorded using the DLS technique. Similar results of the high stability of Ag-Au alloy NPs with 1:3 molar ratio has been reported before [9]. The stability can be attributed to the addition of NH_4OH solution which forms a soluble $[Ag(NH_3)_2]+$ complex with AgCl precipitate. Subsequent addition of $NaBH_4$ helps in the co-reduction of metal ions in the presence of NH_4OH showing a gradual shift in absorption peak that reflects the alloying of gold and silver NPs. For other trials of Ag-Au alloy NPs having 3:1 and 1:1 molar ratio, stability remains crucial parameter. In the case of PVA coated alloy NPs, all the suspensions were stable and did not precipitate. This can be attributed to the polymeric network of PVA in the solution which prevents gold nanoparticles from agglomerating and hence stabilizing the colloidal solution [41].. UV-vis results show formation of alloy NPs evident from the gradual red shift from Ag NP to Au NP in both cases. UV-vis spectra of mechanically mixed pure gold and silver NPs were compared to the synthesized alloy NPs which shows two distinct absorption peaks rather than a single intermediate peak for alloy NPs.

Table 3.5: Hydrodynamic size measurement of pure Ag, pure Au, and Ag-Au alloy NPs@PVA. Alloy NPs were more stable when capped with PVA which stabilize the particles.

Sample	Hydrodynamic Size in number [d.nm] (average of 3)	Standard deviation (average of 3)	(PdI) (average of 3)
Ag	**15**	**4**	**0.472**
Au	**4**	**1**	**0.355**
Ag PVA	**2**	**0.4**	**0.808**
Ag 75 Au 25 PVA	**394**	**87**	**0.728**
Ag 50 Au 50 PVA	**88**	**50**	**0.216**
Ag 25 Au 75 PVA	**54**	**20**	**0.306**
Au PVA	**2**	**0.4**	**0.483**

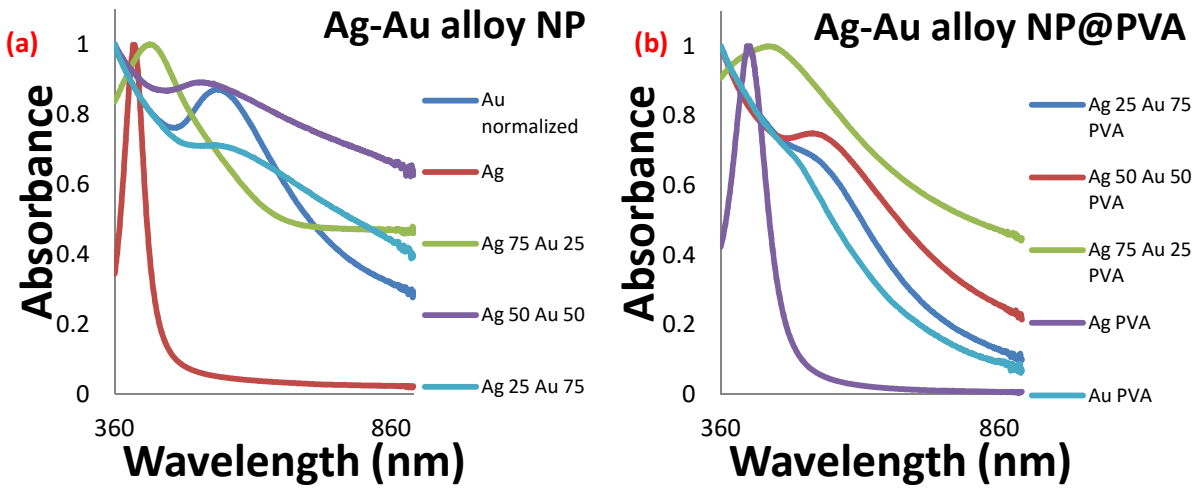

*Fig. 3.17: UV-vis spectra of **(a)** Ag NPs showing little blue shift and **(b)** Au NPs showing a significant blue shift in SPR peak with increasing citrate concentration. Blue shift refers to a decrease in particle size.*

Ag 25 Au 75: The Ag-Au alloy NPs in H20 with 1:3 molar ratio of the silver and gold precursor was chosen for TEM analysis. The sample was dark grey in color and it shows a good stability and transparency. TEM imaging reveals spaghettified NPs chains with small particle diameter in the range 5-10 nm. HRTEM images show NPs of two contrast which can be attributed to homogeneous alloying of Ag-Au NPs.

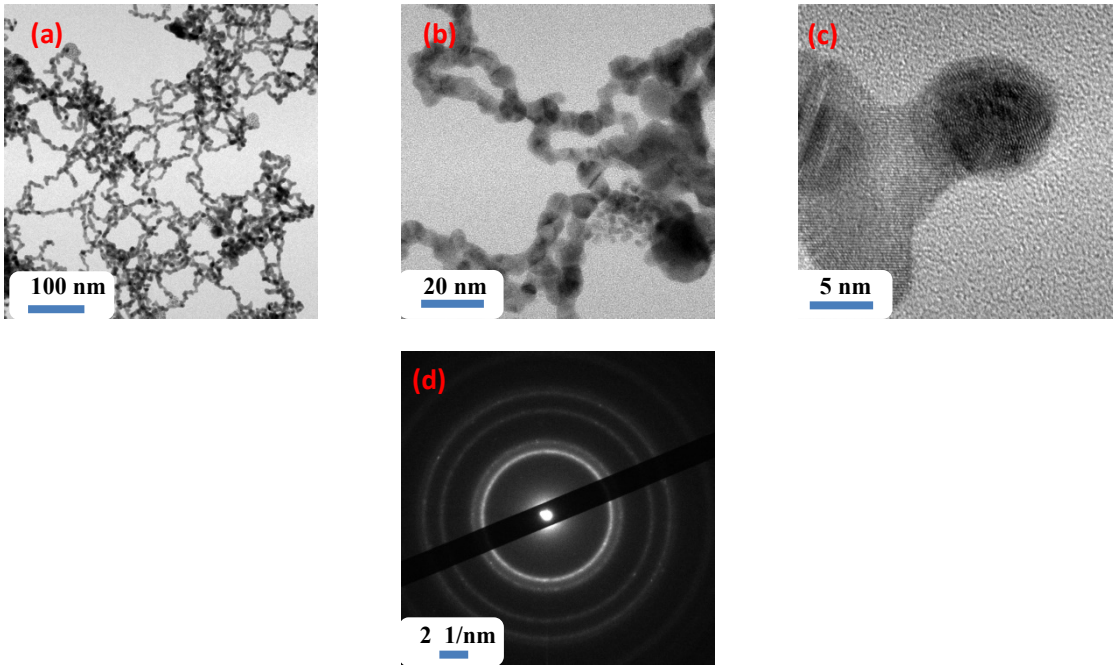

*Fig. 3.18: Representative TEM images of Ag-Au alloy NPs in H_20 with 1:3 molar ratio of the silver and gold precursor at a scale length of **(a)** 100 nm, **(b)** 20 nm, **(c)** 5 nm **(d)** SAED pattern containing diffraction rings of both gold and silver which is hard to discriminate.*

Elemental analysis of homogeneously alloyed Ag-Au NPs:

The elemental composition was determined by EDS mapping of two regions of interest (at 200 nm and 60 nm scale length) as well as point mapping. It confirms the presence of both Ag (blue) and Au (orange) in Ag-Au alloy NPs and gives information about the homogeneity of the alloy NPs. Point mapping reveals the Ag:Au ratio of the alloy NPs is same as in the initial solution.

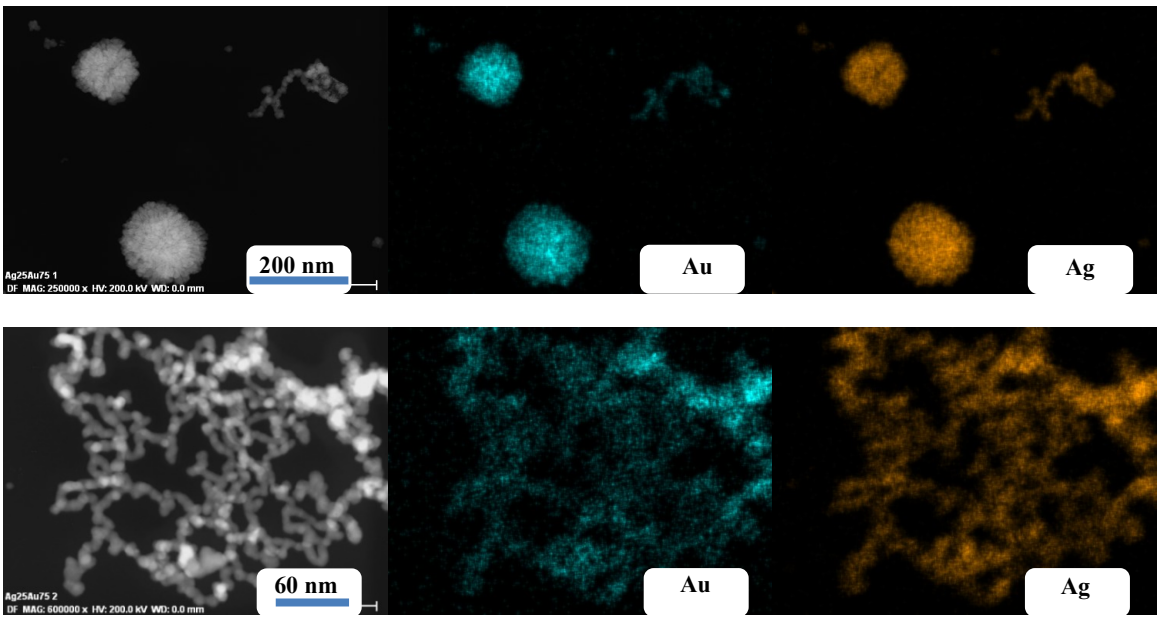

Fig. 3.19: Representative STEM images and EDS mapping of two regions of interest for Ag-Au alloy NPs in H_20 (at 200 nm and 60 nm scale length). Blue color shows the presence of Au and orange color shows the presence of Ag on the mapped homogeneously alloyed gold and silver NPs.

Conclusion

Citrate-stabilized Ag-Au alloy NPs were synthesized by varying the molar ratio of metal precursor in H_20 as well as PVA. The problem of co-reduction of both gold and silver by the strong reducing agent $NaBH_4$ was solved with the addition of NH_4OH which forms a complex with Ag^+ ions. This helps in the formation of homogeneously alloyed Ag-Au NPs. The stability remains a concern. NPs synthesized in H_2O precipitated in a couple of weeks. However, PVA acts as a stabilizing agent and a fine variation in color was observed. Ag 25 Au 75 sample shows a good stability. They were analyzed via TEM and EDS spectroscopy that confirm the formation of homogeneously alloyed NPs.

Overview

In the present thesis, we summarized our recent endeavor towards tailoring shape, size and optical properties of gold and silver nanostructures. Here, we studied the role of various parameter involved in their synthesis with an attempt to develop, optimize and control biocompatible synthesis. Our inability to have a good control on shape and size distribution with a dilution of precursor, possibly because of high metal precursor concentration and low citrate concentration, lead to the formation of NPs of different shapes and sizes. UV-vis spectra show a significant blue shift with a dilution of precursor that suggests a decrease in particle size. TEM images show the formation of NPs of uneven shape and size. Dilution provides more room for NP synthesis and results in uniform dispersion with a poor control on the particle shape and size. To tackle this issue, we devoted our efforts to synthesize spherical NPs (with a core diameter less than 15 nm). The shape and size of metal NPs depends on how effectively they are capped. NPs were synthesized with different citrate concentration which controls the crystallite size and prevent the agglomeration of the NPs. UV-vis spectra show a little red shift for Ag NPs and a significant blue shift for Au NPs with increasing concentration of citrates. TEM analysis clearly shows a great control on particle shape, size and dispersion on increased citrate concentration.

The shift of the SPR peak suggests a change in the particle shape and size which highly depends on the synthesis parameter. Gold and silver nanospheres present a SPR peak at ~415 nm and ~520 nm respectively which are in the visible region. However, introduction of anisotropy leads to a shift in the plasmon band to the NIR region which makes them good candidates for photothermal therapy and bio-medical applications. Au NRs of different aspect ratio were synthesized by varying the concentration of AgNO3. UV-vis spectra show two absorbance peaks, one at ~520 nm in the visible region and the other at 700-1200 nm in the NIR region. TEM analysis confirms an increase of the aspect ratio with increasing AgNO3 concentration.

Finally, the homogeneous alloying of gold and silver NPs is obtained by varying the molar ratio of the metal precursors. This results in intermediate SPR peaks between silver and gold suggesting the formation of alloys. TEM and EDS spectroscopy confirm the formation of homogeneously alloyed NPs.

References:

[1] J. Turkevich, P. C. Stevenson, and J. Hillier, "A study of the nucleation and growth processes in the synthesis of colloidal gold," *Discuss. Faraday Soc.*, vol. 11, no. 0, pp. 55–75, Jan. 1951.

[2] S. Reymond-Laruinaz, L. Saviot, V. Potin, and M. del C. Marco de Lucas, "Protein–nanoparticle interaction in bioconjugated silver nanoparticles: A transmission electron microscopy and surface enhanced Raman spectroscopy study," *Applied Surface Science*, vol. 389, pp. 17–24, Dec. 2016.

[3] M. Jalal *et al.*, "Biosynthesis of Silver Nanoparticles from Oropharyngeal Candida glabrata Isolates and Their Antimicrobial Activity against Clinical Strains of Bacteria and Fungi," *Nanomaterials*, vol. 8, no. 8, p. 586, Aug. 2018.

[4] I. H. El-Sayed, X. Huang, and M. A. El-Sayed, "Surface Plasmon Resonance Scattering and Absorption of anti-EGFR Antibody Conjugated Gold Nanoparticles in Cancer Diagnostics: Applications in Oral Cancer," *Nano Letters*, vol. 5, no. 5, pp. 829–834, May 2005.

[5] J. Rodríguez-Fernández, J. Pérez-Juste, F. J. García de Abajo, and L. M. Liz-Marzán, "Seeded Growth of Submicron Au Colloids with Quadrupole Plasmon Resonance Modes," *Langmuir*, vol. 22, no. 16, pp. 7007–7010, Aug. 2006.

[6] N. R. Jana, L. Gearheart, and C. J. Murphy, "Wet Chemical Synthesis of High Aspect Ratio Cylindrical Gold Nanorods," *The Journal of Physical Chemistry B*, vol. 105, no. 19, pp. 4065–4067, May 2001.

[7] X. Huang, I. H. El-Sayed, W. Qian, and M. A. El-Sayed, "Cancer Cell Imaging and Photothermal Therapy in the Near-Infrared Region by Using Gold Nanorods," *Journal of the American Chemical Society*, vol. 128, no. 6, pp. 2115–2120, Feb. 2006.

[8] P. Dobrowolska, A. Krajewska, M. Gajda-Rączka, B. Bartosewicz, P. Nyga, and B. J. Jankiewicz, "Application of Turkevich Method for Gold Nanoparticles Synthesis to Fabrication of SiO2@Au and TiO2@Au Core-Shell Nanostructures," *Materials*, vol. 8, no. 6, pp. 2849–2862, May 2015.

[9] R. Rajendra, P. Bhatia, A. Justin, S. Sharma, and N. Ballav, "Homogeneously-Alloyed Gold–Silver Nanoparticles as per Feeding Moles," *J. Phys. Chem. C*, vol. 119, no. 10, pp. 5604–5613, Mar. 2015.

[10] "How Much Gold Has Been Mined? | World Gold Council." [Online]. Available: https://www.gold.org/about-gold/gold-supply/gold-mining/how-much-gold-has-been-mined. [Accessed: 07-Aug-2018].

[11] M. Notarianni, K. Vernon, A. Chou, M. Aljada, J. Liu, and N. Motta, "Plasmonic effect of gold nanoparticles in organic solar cells," *Solar Energy*, vol. 106, pp. 23–37, Aug. 2014.

[12] A. Sharma, S. V. Madhunapantula, and G. P. Robertson, "Toxicological considerations when creating nanoparticle based drugs and drug delivery systems?," *Expert Opin Drug Metab Toxicol*, vol. 8, no. 1, pp. 47–69, Jan. 2012.

[13] P. K. Jain, X. Huang, I. H. El-Sayed, and M. A. El-Sayed, "Review of Some Interesting Surface Plasmon Resonance-enhanced Properties of Noble Metal Nanoparticles and Their Applications to Biosystems," *Plasmonics*, vol. 2, no. 3, pp. 107–118, Sep. 2007.

[14] J. Biener, A. Wittstock, T. F. Baumann, J. Weissmüller, M. Bäumer, and A. V. Hamza, "Surface Chemistry in Nanoscale Materials," *Materials*, vol. 2, no. 4, pp. 2404–2428, Dec. 2009.

[15] B. D. Chithrani, A. A. Ghazani, and W. C. W. Chan, "Determining the Size and Shape Dependence of Gold Nanoparticle Uptake into Mammalian Cells," *Nano Letters*, vol. 6, no. 4, pp. 662–668, Apr. 2006.

[16] P. K. Jain, K. S. Lee, I. H. El-Sayed, and M. A. El-Sayed, "Calculated Absorption and Scattering Properties of Gold Nanoparticles of Different Size, Shape, and Composition: Applications in Biological Imaging and Biomedicine," *The Journal of Physical Chemistry B*, vol. 110, no. 14, pp. 7238–7248, Apr. 2006.

[17] G. Schneider, "Antimicrobial silver nanoparticles – regulatory situation in the European Union," *Materials Today: Proceedings*, vol. 4, pp. S200–S207, 2017.

[18] "The Optical Properties of Metal Nanoparticles: The Influence of Size, Shape, and Dielectric Environment - The Journal of Physical Chemistry B (ACS Publications)." [Online]. Available: https://pubs-acs-org.proxy-scd.u-bourgogne.fr/doi/10.1021/jp026731y. [Accessed: 24-Feb-2019].
[19] T. Wriedt, "Mie Theory: A Review," in *The Mie Theory*, vol. 169, W. Hergert and T. Wriedt, Eds. Berlin, Heidelberg: Springer Berlin Heidelberg, 2012, pp. 53–71.
[20] S. K. Ghosh and T. Pal, "Interparticle Coupling Effect on the Surface Plasmon Resonance of Gold Nanoparticles: From Theory to Applications," *Chem. Rev.*, vol. 107, no. 11, pp. 4797–4862, Nov. 2007.
[21] V. Amendola, R. Pilot, M. Frasconi, O. M. Maragò, and M. A. Iatì, "Surface plasmon resonance in gold nanoparticles: a review," *Journal of Physics: Condensed Matter*, vol. 29, no. 20, p. 203002, Apr. 2017.
[22] V. Wagner, A. Dullaart, A.-K. Bock, and A. Zweck, "The emerging nanomedicine landscape," *Nature Biotechnology*, vol. 24, no. 10, pp. 1211–1217, Oct. 2006.
[23] K.-S. Lee and M. A. El-Sayed, "Gold and Silver Nanoparticles in Sensing and Imaging: Sensitivity of Plasmon Response to Size, Shape, and Metal Composition," *J. Phys. Chem. B*, vol. 110, no. 39, pp. 19220–19225, Oct. 2006.
[24] G. FRENS, "Controlled Nucleation for the Regulation of the Particle Size in Monodisperse Gold Suspensions," *Nature Physical Science*, vol. 241, p. 20, Jan. 1973.
[25] D. T. Nguyen, D.-J. Kim, and K.-S. Kim, "Controlled synthesis and biomolecular probe application of gold nanoparticles," *Micron*, vol. 42, no. 3, pp. 207–227, Apr. 2011.
[26] P. Zhao, N. Li, and D. Astruc, "State of the art in gold nanoparticle synthesis," *Coordination Chemistry Reviews*, vol. 257, no. 3–4, pp. 638–665, Feb. 2013.
[27] C. J. Orendorff and C. J. Murphy, "Quantitation of Metal Content in the Silver-Assisted Growth of Gold Nanorods," *J. Phys. Chem. B*, vol. 110, no. 9, pp. 3990–3994, Mar. 2006.
[28] P. V. Kamat, M. Flumiani, and G. V. Hartland, "Picosecond Dynamics of Silver Nanoclusters. Photoejection of Electrons and Fragmentation," *The Journal of Physical Chemistry B*, vol. 102, no. 17, pp. 3123–3128, Apr. 1998.
[29] J. Stetefeld, S. A. McKenna, and T. R. Patel, "Dynamic light scattering: a practical guide and applications in biomedical sciences," *Biophysical reviews*, vol. 8, no. 4, pp. 409–427, Oct. 2016.
[30] M. Schulz-Dobrick, K. V. Sarathy, and M. Jansen, "Surfactant-Free Synthesis and Functionalization of Gold Nanoparticles," *J. Am. Chem. Soc.*, vol. 127, no. 37, pp. 12816–12817, Sep. 2005.
[31] C. J. Murphy *et al.*, "Gold Nanoparticles in Biology: Beyond Toxicity to Cellular Imaging," *Acc. Chem. Res.*, vol. 41, no. 12, pp. 1721–1730, Dec. 2008.
[32] B. Viswanath, P. Kundu, A. Halder, and N. Ravishankar, "Mechanistic Aspects of Shape Selection and Symmetry Breaking during Nanostructure Growth by Wet Chemical Methods," *J. Phys. Chem. C*, vol. 113, no. 39, pp. 16866–16883, Oct. 2009.
[33] J. Polte *et al.*, "Mechanism of Gold Nanoparticle Formation in the Classical Citrate Synthesis Method Derived from Coupled In Situ XANES and SAXS Evaluation," *J. Am. Chem. Soc.*, vol. 132, no. 4, pp. 1296–1301, Feb. 2010.
[34] L. Maurizi, F. Bouyer, J. Paris, F. Demoisson, L. Saviot, and N. Millot, "One step continuous hydrothermal synthesis of very fine stabilized superparamagnetic nanoparticles of magnetite," *Chemical Communications*, vol. 47, no. 42, p. 11706, 2011.
[35] J. Polte *et al.*, "Nucleation and Growth of Gold Nanoparticles Studied via in situ Small Angle X-ray Scattering at Millisecond Time Resolution," *ACS Nano*, vol. 4, no. 2, pp. 1076–1082, Feb. 2010.
[36] J. M. Luther, P. K. Jain, T. Ewers, and A. P. Alivisatos, "Localized surface plasmon resonances arising from free carriers in doped quantum dots," *Nature Materials*, vol. 10, p. 361, Apr. 2011.
[37] C. J. Murphy *et al.*, "Anisotropic Metal Nanoparticles: Synthesis, Assembly, and Optical Applications," *J. Phys. Chem. B*, vol. 109, no. 29, pp. 13857–13870, Jul. 2005.

[38] L. M. Liz-Marzán, “Tuning nanorod surface plasmon resonances | SPIE Homepage: SPIE.” [Online]. Available: http://spie.org/newsroom/0798-tuning-nanorod-surface-plasmon-resonances. [Accessed: 25-Mar-2019].
[39] D. K. Smith and B. A. Korgel, “The Importance of the CTAB Surfactant on the Colloidal Seed-Mediated Synthesis of Gold Nanorods,” *Langmuir*, vol. 24, no. 3, pp. 644–649, Feb. 2008.
[40] L. M. Liz-Marzán, “Tailoring Surface Plasmons through the Morphology and Assembly of Metal Nanoparticles,” *Langmuir*, vol. 22, no. 1, pp. 32–41, Jan. 2006.
[41] P. Adhyapak *et al.*, “Thickness-dependent humidity sensing by poly(vinyl alcohol) stabilized Au–Ag and Ag–Au core–shell bimetallic nanomorph resistors,” *Royal Society Open Science*, vol. 5, no. 6, p. 171986, Jun. 2018.